bioRxiv preprint doi: https://doi.org/10.1101/2024.06.19.599732; this version posted June 28, 2025. The copyright holder for this preprint (which was not certified by peer review) is the author/funder, who has granted bioRxiv a license to display the preprint in perpetuity. It is made available under aCC-BY-NC 4.0 International license.

Mouse models of non-dystrophic and dystrophic myotonia exhibit nociplastic pain-like behaviors

Tyler S. Nelson[1], Aida Calderon-Rivera[1], Heather N. Allen[1], Emanuel Loeza-Alcocer[2], Jorge B. Pineda-Farias[2], Narges Pachenari[2], Kimberly Gomez[1], Santiago Loya-Lopez[1], Erick J. Rodriguez-Palma[1], Paz Duran[3], Michael S. Gold[2], Rajesh Khanna[1*]

1. Department of Pharmacology and Therapeutics, McKnight Brain Institute, and Center for Advanced Pain Therapeutics and Research (CAPToR), College of Medicine, University of Florida, Gainesville, FL 32610, USA
2. Department of Neurobiology, and Pittsburgh Center for Pain Research, School of Medicine, University of Pittsburgh, Pittsburgh, PA, 15261
3. Department of Molecular Pathobiology, College of Dentistry, New York University, New York, NY 10010, USA

***Corresponding author**:
Name: Rajesh Khanna, Ph.D.
Mailing Address: 1149 Newell Drive, Room, Gainesville, FL 32610, USA
Email: r.khanna@ufl.edu

Conflicts of Interest: R.K. is the founder of Regulonix LLC, a company developing non-opioids drugs for chronic pain.

bioRxiv preprint doi: https://doi.org/10.1101/2024.06.19.599732; this version posted June 28, 2025. The copyright holder for this preprint (which was not certified by peer review) is the author/funder, who has granted bioRxiv a license to display the preprint in perpetuity. It is made available under aCC-BY-NC 4.0 International license.

Abstract

Pain is a prominent and debilitating symptom in myotonic disorders, including myotonia congenita and myotonic dystrophy type 1 (DM1). Although patients frequently report chronic pain, its underlying mechanisms remain poorly defined. In both disorders, impaired chloride conductance through voltage-gated CLC-1 chloride channels in skeletal muscle disrupts membrane repolarization, leading to delayed relaxation and persistent muscle hyperexcitability. Here, we investigated the pathophysiology of pain in mouse models of acute and chronic myotonia. In the acute model, a single intraperitoneal injection of anthracene-9-carboxylic acid (9-AC, 30 mg/kg), a selective ClC-1 antagonist, induced transient muscle stiffness, cramping, and gait abnormalities, followed by prolonged pain-like behavior, including static and dynamic mechanical allodynia, thermal hyperalgesia, and cold hypersensitivity for up to 48 hours. Whole-cell patch-clamp recordings from dorsal root ganglion neurons demonstrated increased action potential firing in small diameter sensory neurons, consistent with enhanced peripheral excitability of putative nociceptors. Compound action potentials from isolated sciatic nerves revealed that 9-AC impaired A-fiber recruitment and stimulus-response gain without affecting conduction velocity, suggesting a reduction in non-nociceptive fiber input that may disinhibit central nociceptive processing. To assess central mechanisms of sensitization, we performed *in vivo* fiber photometry of the parabrachial nucleus (PBN), a key supraspinal hub for pain signaling. Mice treated with 9-AC exhibited exaggerated PBN responses to normally innocuous mechanical and cold stimuli, indicative of enhanced central nociceptive transmission. Having established that acute myotonia can evoke both peripheral and central sensitization, we next examined whether chronic myotonic activity in a disease-relevant genetic model produces similar pathophysiological changes. To model chronic myotonia, we evaluated HSA LR20b mice, a transgenic model of DM1 carrying a skeletal muscle-specific CTG repeat expansion. These mice displayed persistent mechanical and thermal hypersensitivity, along with elevated dorsal root ganglia neuron excitability, supporting sustained peripheral sensitization in a genetic model of myotonic disease. Together, these findings establish robust preclinical models of myotonic pain and demonstrate that myotonia drives a prolonged nociplastic pain state through combined peripheral and central mechanisms. These results provide a foundation for future studies aimed at identifying and validating therapeutic targets for pain associated with myotonic disorders.

bioRxiv preprint doi: https://doi.org/10.1101/2024.06.19.599732; this version posted June 28, 2025. The copyright holder for this preprint (which was not certified by peer review) is the author/funder, who has granted bioRxiv a license to display the preprint in perpetuity. It is made available under aCC-BY-NC 4.0 International license.

Introduction

Myotonic disorders are inherited neuromuscular conditions characterized by delayed muscle relaxation following voluntary contraction[1,2]. This defining feature, known as myotonia, arises from increased skeletal muscle excitability and is most commonly caused by mutations in *CLCN1* and *SCN4A*, which encode the skeletal muscle chloride channel CLC-1 and the voltage-gated sodium channel $Na_V1.4$, respectively[3,4]. Clinically, myotonia may manifest as overt muscle stiffness or as more subtle impairments in muscle relaxation detectable only through electromyography (EMG)[3,5,6]. These symptoms frequently interfere with motor function, elevate fall risk, and substantially reduce quality of life[7-9].

CLC-1 plays a central role in stabilizing skeletal muscle excitability by facilitating chloride ion conductance across the sarcolemma[10]. Loss-of-function mutations in *CLCN1* impair chloride conductance, resulting in sustained depolarization and delayed repolarization of muscle fibers[11]. This pathomechanism underlies both autosomal dominant (Thomsen's disease) and autosomal recessive (Becker's disease) forms of myotonia congenita[12-15]. A similar mechanism contributes to myotonia in myotonic dystrophy type 1 (DM1), where mis-splicing of *CLCN1* mRNA leads to reduced CLC-1 expression and subsequent muscle hyperexcitability[16-18].

To investigate myotonia in experimental conditions, researchers have long employed monocarboxylic aromatic acids, which reliably induce muscle stiffness and characteristic EMG abnormalities in mammalian and amphibious skeletal muscle[19-27]. Among these compounds, anthracene-9-carboxylic acid (9-AC) is one of the most widely used and well-characterized agents. By selectively blocking CLC-1 channels[21,28-30], 9-AC rapidly induces myotonic symptoms across multiple species, including rodent[31-34], rabbit[30], goat[21], canine[35], porcine[36], and human skeletal muscle[37,38]. In rodents, systemic administration of 9-AC produces robust, transient muscle hyperexcitability and has become a standard pharmacological tool for evaluating candidate anti-myotonic therapies *in vivo*[31,32,39-41].

Although the electrophysiological basis of myotonia has been extensively studied, its contribution to the pathophysiology of pain remains poorly understood. Historically, myotonic disorders have been conceptualized as skeletal muscle channelopathies, yet pain has long been described as a prominent and distressing symptom. Early accounts from the late 19th century document severe, recurring muscle pain in affected individuals. In an 1886 article published in *Brain*, Dr. White described a patient whose "cramps caused great pain, and came on several times a day, and lasted a long while[42]." Dana (1888) reported that patients "complain bitterly at times of aching pains in the legs[43]," while Deligny (1885) observed muscle contractions "always accompanied with such violent pain that the patient would roll on the earth in his agony[44,45]." These descriptions illustrate that pain has historically been recognized as a consistent and debilitating feature of the myotonic phenotype. Contemporary studies reinforce these observations[46,47]. Patients with myotonia congenita[8,48-51], myotonic dystrophies (DM1 and DM2)[52-59], and *SCN4A*-related

bioRxiv preprint doi: https://doi.org/10.1101/2024.06.19.599732; this version posted June 28, 2025. The copyright holder for this preprint (which was not certified by peer review) is the author/funder, who has granted bioRxiv a license to display the preprint in perpetuity. It is made available under aCC-BY-NC 4.0 International license.

myotonic disorders[46,60-65] frequently report high-impact, treatment-resistant muscle pain that substantially limits daily functioning and is often the primary motivation for seeking medical care[7,46,47,54,55,66-69]. However, despite its prevalence and clinical relevance, the mechanistic basis of pain in myotonic disorders remains completely unknown, and no targeted analgesic treatments currently exist.

Given this gap in knowledge and the historical and clinical evidence of pain in myotonic disorders, we hypothesized that muscle membrane hyperexcitability may itself be sufficient to trigger persistent pain-like states. To test this, we employed both pharmacological (9-AC) and genetic (DM1) models of myotonia to evaluate whether muscle hyperexcitability alone is sufficient to drive pain. We show that a single episode of 9-AC-induced myotonia evokes prolonged mechanical, thermal, and cold hypersensitivity, alongside increased excitability of peripheral sensory neurons and amplified central nociceptive signaling. These findings establish a mechanistic link between myotonia and pain, suggesting that muscle hyperexcitability is not only a hallmark of motor dysfunction, but also a direct driver of nociplastic pain.

bioRxiv preprint doi: https://doi.org/10.1101/2024.06.19.599732; this version posted June 28, 2025. The copyright holder for this preprint (which was not certified by peer review) is the author/funder, who has granted bioRxiv a license to display the preprint in perpetuity. It is made available under aCC-BY-NC 4.0 International license.

Methods

Animals

Adult C57Bl/6J (Jackson Laboratory, # 000664), FVB/NJ (Jackson Laboratory, # 001800) and (FVB/N-Tg(HSA*LR)20bCath/J (Jackson Laboratory #032031) male and female mice were group housed, provided access to food and water *ad libitum*, and maintained on a 12:12 hour light:dark cycle in temperature and humidity-controlled rooms. Equal numbers of male and female mice were used in all experiments. Although we were not powered to detect significant sex differences, no major/obvious trends in sex differences were observed and means from both sexes were pooled. All procedures were consistent with the guidelines for the treatment of animals of the International Association for the Study of Pain and were approved by the University of Florida's and the University of Pittsburgh's Institutional Animal Care and Use Committee.

Drug Administration

Anthracene-9-carboxylic acid, 99% purity (Thermo Scientific, Cat# 104880100), was diluted in a solution containing 50% dimethyl sulfoxide and 50% sterile 0.9% sodium chloride, while the vehicle comprised the same constituents. The drug was freshly prepared each day just before administration due to its tendency to precipitate out of solution rapidly. Mice were briefly scruffed and received a single intraperitoneal (i.p.) injection using a 30-gauge needle.

Electrophysiological recordings in sensory neurons

Whole-cell patch-clamp recordings were performed in dissociated dorsal root ganglion (DRG) neurons, following protocols previously established by our group[70,71]. Lumbar DRGs were harvested from adult male and female mice (9 weeks to 3 months old). For 9-AC recordings, DRG isolation occurred either 6 hours (for recordings at 24 hours post-9-AC injection) or 24 hours (for recordings at 48 hours post-injection) after administration of 9-AC (30 mg/kg, i.p.). DRG tissues were enzymatically dissociated at 37°C for 50 minutes in Dulbecco's Modified Eagle Medium (DMEM) containing collagenase type I (1.66 mg/mL, Cat# LS004194; Worthington) and neutral protease (1.04 mg/mL, Cat# LS02104; Worthington). Following centrifugation (800 rpm, 5 minutes), dissociated neurons were plated onto 12-mm poly-D-lysine-coated coverslips (0.1 mg/mL, Cat# P6407; Millipore Sigma) and maintained in culture medium supplemented with 10% fetal bovine serum (HyClone) and 1% penicillin/streptomycin (Cat# 15140; Life Technologies). Electrophysiological recordings were conducted 15-24 hours after plating using the whole-cell configuration of the patch-clamp technique in current-clamp mode. Recordings were performed at room temperature (20-22°C) using an EPC 10 amplifier (HEKA Elektronik, Germany) and acquired with PatchMaster. The data analysis was done with FitMaster and Easy Electrophysiology softwares. Borosilicate glass pipettes (resistance ~2-3.5 MΩ) were filled with internal solution (see below) and giga-ohm seals were formed with DRG neurons. Borosilicate glass pipettes (resistance ~2-3.5 MΩ) were filled with internal solution (see below) and giga-ohm seals were formed with DRG neurons. After achieving the whole-cell configuration under voltage clamp, recordings were switched to current-clamp mode to assess neuronal excitability.

bioRxiv preprint doi: https://doi.org/10.1101/2024.06.19.599732; this version posted June 28, 2025. The copyright holder for this preprint (which was not certified by peer review) is the author/funder, who has granted bioRxiv a license to display the preprint in perpetuity. It is made available under aCC-BY-NC 4.0 International license.

Neurons were categorized as small (<15 pF and diameter under 23 μm) or large (>40 pF and diameter ~37 μm) based on measured whole-cell capacitance and approximate size. In small-diameter neurons (capacitance <15 pF), action potentials (APs) were elicited with a depolarizing ramp protocol (0-150 or 0-250 pA over 1 second for DM1 mice or 9-AC treatment, respectively), and rheobase was calculated as the minimal current required to evoke an AP. In contrast, large-diameter neurons (average capacitance ~45 pF) were not amenable to ramp protocols due to intrinsic membrane properties. Specifically, their larger capacitance and differential channel expression reduce the rate of membrane depolarization during ramps, leading to depolarization-induced inactivation and failure to generate APs. Therefore, in large neurons, rheobase was determined using step current injections starting at 0 pA and increasing in 100 pA increments (1-second duration per step).

Table 1: Solutions for Electrophysiological Recordings	
External solution for small and large DRG neurons (in mM)	130 NaCl, 3 KCl, 2.5 $CaCl_2$, 0.6 $MgCl_2$, 10 HEPES, 10 Glucose (pH adjusted to 7.4)
Internal solution for small DRG neurons (in mM)	120 K-gluconate, 10 NaCl, 4 Mg-ATP, 10 HEPES, 5 EGTA, 2 $MgCl_2$ (pH adjusted to 7.2)
Internal solution for large DRG neurons (in mM)	110 K-methanesulfonate, 30 KCl, 5 NaCl, 1 $CaCl_2$, 2 $MgCl_2$, 2 Mg-ATP, 1 Li-GTP, 10 HEPES, 11 EGTA (pH adjusted to 7.2)

Compound Action Potentials

For compound action potential (CAP) recording, sciatic nerves, from the trifurcation to the iliac crest, were removed bilaterally after mice had been deeply anesthetized with isoflurane and perfused transcardially with ice cold 0.1 M phosphate buffered saline. Nerves were place in oxygenated Kreb's solution (136 NaCl, 5.6 KCl, 14.3 NaHCO3, 1.2 NaH2PO4, 2.2 CaCl2, 1.2 MgCl2, and 11 glucose bubbled continuously with carbogen (O2 95%/CO2 5%) to achieve a pH ranging from 7.2 to 7.4.) and stored on ice until recording. Glass section electrodes were used for both stimulation (at the distal end) and recording (at the proximal end), where an amplifier (A-M Systems, Inc Sequim WA) was used to deliver square pulse of 0.3 (A-wave) and 3 ms (C-wave) to the nerve. The CAP recording electrode was connected to a differential preamplifier (0.1-10 kHz; model DAM-80, WPI), and the recording was sampled at 20 kHz via a Molecular Devices Digidata (1440a) analog-to-digital converter and acquired and analyzed using pCLAMP version 10 for MS Windows (Molecular Devices, San Jose CA). After mounting the nerve in the recording chamber, it was given 30 minutes to settle prior to further study. Recordings were performed at room temperature.

For each nerve, the A-wave, component of the CAP conducting at >6 m/s) was studied first. The threshold was defined as the current intensity required to evoke a deflection in the voltage trace >3x the baseline

bioRxiv preprint doi: https://doi.org/10.1101/2024.06.19.599732; this version posted June 28, 2025. The copyright holder for this preprint (which was not certified by peer review) is the author/funder, who has granted bioRxiv a license to display the preprint in perpetuity. It is made available under aCC-BY-NC 4.0 International license.

noise in the voltage trace (taken 10 seconds prior to stimulation). A recruitment curve was then generated by stimulating the nerve at 1.5, 2, 3, 4, 5, 10, and 20x threshold. A 10 second inter-stimulus interval was used. The nerve was then stimulated 20 times at 10x threshold intensity at 30 Hz and 100 Hz to assess activity dependent changes in the waveform. The C-wave was then studied with the same criteria used to determine the threshold for the activation of fibers conducting at <2 ms. A recruitment curve was then generated by stimulating the nerve at 1.5, 2, and 3x threshold.

Conduction velocity was estimated based on the length of the nerve divided by latency of the peak of the rectified A- and C-waves relative to the initiation of the stimulation artifact. The integral (Area under the curve, AUC) of the rectified waveform evoked in response to each stimulus was used to generate recruitment curves. The AUC of the waveform evoked with the 20th pulse divided by that of the first pulse was used to estimate activity dependent changes in the CAP A-wave. Recruitment curves for the A-wave of the CAP were fitted with a logistic equation, f(x) = (AUCmax*x^slope)/(x^slope+AUC50^slope) that enabled estimation of the maximal AUC (AUCmax), current intensity associated with the activation of a CAP 50% of maximal (AUC50), and the slope of the curve at the 50% point.

Fiber Photometry Recordings

As previously described by our group[70,72-74], adult male and female wild-type mice received unilateral stereotaxic injections of 300 nL AAV9-CaMKIIa-GCaMP6s-WPRE-SV40 (Addgene, Watertown, MA) into the right parabrachial nucleus (PBN) to selectively express the calcium indicator GCaMP6s in glutamatergic neurons. Stereotaxic coordinates targeting the PBN were anteroposterior (AP) −5.15 mm, mediolateral (ML) ±1.45 mm, and dorsoventral (DV) −3.45 mm from bregma. Viral infusions were performed using a Nanoject II Auto-Nanoliter Injector (Drummond) at a rate of 2 nL/sec, with a post-infusion dwell time of 5 minutes to minimize reflux. Immediately following viral delivery, a fiber optic cannula (RWD; 1.25 mm ferrule diameter, 200 µm core diameter, 0.37 numerical aperture) was chronically implanted above the injection site and secured with dental cement (Cat# 10-000-786, Stoelting, Wood Dale, IL). Mice were allowed to recover for 21 days to allow for robust viral expression. Prior to each recording session, animals were acclimated in acrylic chambers with wire mesh flooring for a minimum of one hour, with the fiber optic patch cord connected and the experimenter in the room. Real-time calcium signals were acquired using the FP3002 fiber photometry system (Neurophotometrics). The plantar surface of the left hindpaw was sequentially stimulated with four sensory stimuli: a 0.07 g von Frey filament (1-second application), a 1.0 g von Frey filament (1-second application), a 10 µL acetone drop, and a blunt pinprick. Each stimulus was presented three times at 2-minute intervals, and the three trials were averaged to represent each animal's response. Calcium signals were analyzed using custom MATLAB scripts. The 470 nm GCaMP6s signal was normalized to the 405 nm isosbestic control channel to correct for motion artifacts and photobleaching. The change in fluorescence (ΔF/F) was calculated by subtracting the baseline signal (10 seconds prior to stimulus onset) from the peak response following stimulation. Area under the curve (AUC) was computed

bioRxiv preprint doi: https://doi.org/10.1101/2024.06.19.599732; this version posted June 28, 2025. The copyright holder for this preprint (which was not certified by peer review) is the author/funder, who has granted bioRxiv a license to display the preprint in perpetuity. It is made available under aCC-BY-NC 4.0 International license.

for the 10-second window following each stimulus. Following baseline recordings, mice received a single intraperitoneal injection of either vehicle or 9-AC (30 mg/kg). Recordings were repeated 24 hours later to assess changes in PBN activity. A crossover design was employed such that, after a one-month washout, the same animals received the alternate treatment and underwent a second round of photometry recordings. Upon completion of the study, animals were deeply anesthetized and transcardially perfused with ice-cold 1x PBS followed by 10% neutral buffered formalin (Cat# SF98-4, Fisher Scientific, Waltham, MA). Brains were extracted, post-fixed, cryoprotected, and coronally sectioned at 30 µm thickness using a cryostat. Sections were stored at 4°C until further processing. To verify GCaMP6s expression and fiber placement, immunohistochemistry for GFP was performed. Sections were washed three times in PBS, blocked in 5% normal goat serum (NGS) in PBS with 0.1% Triton X-100 for one hour, and incubated overnight at room temperature with rabbit anti-GFP (1:1000; Cat# AB3080, Millipore Sigma, St. Louis, MO) in blocking buffer. After washing, sections were incubated for 1.5 hours in goat anti-rabbit AlexaFluor 488 secondary antibody (Cat# A11008, Invitrogen, Waltham, MA), washed again, mounted on SuperFrost Plus microscope slides (Cat# 22-037-246, Fisher Scientific), and coverslipped using Vectashield Plus antifade mounting medium with DAPI (H-2000-10, Vector Laboratories). Images were acquired using a Leica DMi8 inverted widefield fluorescence microscope at 20x magnification. No animals were excluded based on post hoc verification of viral transfection or fiber placement.

Behavioral Testing

Static Mechanical Sensitivity (von Frey): Testing was performed as previously described[70,75,76]. Mice were habituated to plexiglass chambers (80 × 80 × 110 mm) on a raised wire mesh platform for 60 minutes immediately prior to behavioral testing. Testing was performed using a calibrated set of logarithmically increasing von Frey monofilaments (Braintree Scientific Cat# 58011) that range in gram force from 0.007 to 6.0 g. Beginning with a 0.4 g filament, these were applied perpendicular to the lateral hindpaw surface with sufficient force to cause a slight bending of the filament. A positive response was denoted as a rapid withdrawal of the paw within 4 seconds of application and was followed by application of the next lower filament. A negative response was followed by application of the next higher filament. An up-down method [77] was used to calculate the 50% withdrawal threshold for each mouse.

Dynamic Mechanical Sensitivity (Brush): Immediately following von Frey testing, dynamic mechanical sensitivity testing was performed on mice in the same plexiglass chambers on a raised wire mesh platform. A cotton swab was “puffed-out” to about three times its original size. The left hindpaw was then brushed using this cotton swab in the heel-to-toe direction. A positive response was noted as a rapid withdrawal of the paw in response to stimulation. The test was repeated four times, and the frequency of responses was reported.

bioRxiv preprint doi: https://doi.org/10.1101/2024.06.19.599732; this version posted June 28, 2025. The copyright holder for this preprint (which was not certified by peer review) is the author/funder, who has granted bioRxiv a license to display the preprint in perpetuity. It is made available under aCC-BY-NC 4.0 International license.

Cool Withdrawal Duration (Acetone): Testing was performed as previously described[70,75,76]. Immediately following dynamic brush testing, sensitivity to non-noxious cold testing was performed on mice in the same plexiglass chambers on a raised wire mesh platform. Using a syringe connected to PE-90 tubing, flared at the tip to a diameter of 3 1/2 mm, we applied a drop of acetone (VWR Cat# BDH1101-1LP) to the plantar surface of the hind left paw. Surface tension maintained the volume of the drop to ~10 μL. The duration of time the animal lifted or shook its paw was recorded for 30 seconds. Three observations were averaged.

Time to Righting Reflex (TRR): Mice were gently placed on their backs on a flat surface to initiate the test. The duration it took for the mouse to return to an upright position, termed the righting reflex, was recorded. Each trial was repeated three times at each time point, and the average of these observations was calculated. This reflex serves as an indicator of the mouse's motor coordination and recovery capability. In healthy mice, the time to right for all animals was less than 0.5 seconds making variability smaller than could be plotted.

Thermal Withdrawal Threshold (Hot/Cold Plate): We evaluated acute nociceptive responses with a hot plate as previously described[76,78,79]. Briefly, prior to testing mice acclimated to the testing room for at least 30 minutes to minimize stress-induced behaviors. Following acclimation, mice were gently placed on a 0-55 °C Ugo Basile hot/cold plate (Stoelting Cat:55075). The trial ended when the mouse exhibited a nociceptive response (such as paw licking or jumping) or after a cutoff time of 30 seconds if no response was observed. Testing was repeated for 3 trials per mouse per temperature with intervals of at least 10 minutes between each trial. The latency to respond for each trial was averaged to produce the mean latency for statistical analysis.

Blinding and Randomization

Rigorous efforts were made to ensure blinding and reduce bias throughout all experiments. For studies involving 9-AC, experimenters were blinded to treatment condition (vehicle vs. 9-AC) during behavioral testing, fiber photometry recordings, and electrophysiological assessments. In experiments using the HSA LR20b transgenic mouse model of DM1, experimenters were blinded to genotype (wild-type vs. DM1) for both behavioral assays and electrophysiological recordings. Animals were randomly assigned to treatment or genotype groups, and data collection and analysis were conducted without knowledge of group allocation until after the completion of experiments.

Statistics, Graphics, and Data Availability

All data are expressed as mean ± standard error of the mean (SEM), with individual data points representing either single animals (for behavioral and fiber photometry studies) or individual neurons (for electrophysiological experiments). Statistical analyses were performed using GraphPad Prism (v10.2.3). Comparisons between two groups were conducted using unpaired two-tailed Student's *t* test for normally

bioRxiv preprint doi: https://doi.org/10.1101/2024.06.19.599732; this version posted June 28, 2025. The copyright holder for this preprint (which was not certified by peer review) is the author/funder, who has granted bioRxiv a license to display the preprint in perpetuity. It is made available under aCC-BY-NC 4.0 International license.

distributed data, or Mann-Whitney *U* test for nonparametric comparisons as appropriate. For time course data, two-way repeated-measures ANOVA was used, followed by Holm-Sidak's or Sidak's multiple comparisons post hoc tests. One-way ANOVA with Dunnett's post hoc test was used for fiber photometry comparisons across multiple stimuli. Area under the curve (AUC) values were calculated using the trapezoidal rule. *p* values less than 0.05 were considered statistically significant. No formal power analysis was conducted. Sample sizes were based on prior experience with similar behavioral and electrophysiological assays. Group sizes, exact *n* values, and statistical tests used are detailed in the figure legends. Figures were generated using Prism, Adobe Illustrator 2022, and Biorender.com and all graphical illustrations were designed to clearly represent individual data variability alongside group averages. All data supporting the findings of this study are available from the corresponding author upon reasonable request. No custom code was generated.

bioRxiv preprint doi: https://doi.org/10.1101/2024.06.19.599732; this version posted June 28, 2025. The copyright holder for this preprint (which was not certified by peer review) is the author/funder, who has granted bioRxiv a license to display the preprint in perpetuity. It is made available under aCC-BY-NC 4.0 International license.

Results

Anthracene-9-carboxylic acid (9-AC) produces transient myotonia and persistent pain-like behavior in mice.

To model an acute myotonic episode, we administered a single intraperitoneal injection of the ClC-1 antagonist, anthracene-9-carboxylic acid (9-AC; 30 mg/kg[31]). As illustrated in **Figure 1A**, we used the righting reflex assay to quantify muscle hyperexcitability following drug administration, a validated measure of myotonia based on delayed recovery from forced supine positioning[31,32]. Consistent with previous reports in both mice[39] and rats[31,34], 9-AC rapidly induced symptoms of muscle stiffness, impaired gait, and delayed movement initiation. Importantly, no sedation, respiratory suppression, or altered consciousness were observed. Quantification of the time to righting reflex (TRR) revealed a significant delay in 9-AC-treated animals compared to vehicle-injected controls, confirming successful induction of transient myotonia (**Figure 1B-C**).

To determine whether this transient myotonia was sufficient to produce pain-like behavior, we performed longitudinal nociceptive testing over a 72-hour period following injection **(Figure 2A)**. Mice treated with 9-AC developed robust hypersensitivity across multiple sensory modalities. Compared to vehicle controls, 9-AC-treated mice exhibited reduced mechanical withdrawal thresholds **(Figure 2B-C)**, increased responsiveness to light brushing **(Figure 2D-E)**, and exaggerated flinching in response to acetone application **(Figure 2F-G)**, indicating the development of static mechanical allodynia, dynamic mechanical allodynia, and cold allodynia, respectively. In addition, 9-AC induced thermal hyperalgesia, as measured by reduced withdrawal latency on the 52 °C hot plate test **(Figure 2H-I)**. These hypersensitivity phenotypes were evident as early as 6 hours post-injection and persisted for up to 48 hours, even though motor symptoms fully resolved by approximately 3 hours post-injection (**Figure 1B**). Together, these findings demonstrate that a single, transient episode of myotonia is sufficient to initiate a prolonged pain-like behavior state consistent with a nociplastic pain phenotype.

9-AC increases excitability of small-diameter dorsal root ganglion (DRG) neurons

We next examined the neural mechanisms underlying 9-AC-induced pain-like behavior. Given that pain is driven by peripheral and/or central sensitization of nociceptive pathways[80,81], we hypothesized that transient myotonia promotes peripheral sensitization through increased excitability of primary afferent or sensory neurons, whose cell bodies are housed in DRGs. To assess this, we performed whole-cell patch-clamp recordings from neurons dissociated from lumbar DRGs, 24 hours after 9-AC injection **(Figure 3A)**. DRGs were harvested 6 hours after injection and maintained in culture until the time of recording. Representative current-clamp traces revealed increased action potential (AP) firing in small-diameter neurons from 9-AC-treated mice compared to vehicle controls **(Figure 3B)**. Quantification showed no difference in resting membrane potential **(Figure 3C)** or rheobase **(Figure 3D)**, but 9-AC increased the number of evoked APs **(Figure 3E)**, indicating enhanced excitability.

bioRxiv preprint doi: https://doi.org/10.1101/2024.06.19.599732; this version posted June 28, 2025. The copyright holder for this preprint (which was not certified by peer review) is the author/funder, who has granted bioRxiv a license to display the preprint in perpetuity. It is made available under aCC-BY-NC 4.0 International license.

To determine whether this increased sensory neuron excitability persisted beyond 24 hours, we performed a second set of recordings 48 hours after 9-AC injection (**Supplemental Figure 1A**). At this later time point, representative traces (**Supplemental Figure 1B**) and quantification of resting membrane potential (**Supplemental Figure 1C**), rheobase (**Supplemental Figure 1D**), and evoked APs (**Supplemental Figure 1E**) showed no significant differences between groups. These electrophysiological findings align with behavioral results showing resolution of mechanical and thermal hypersensitivity by 48 hours post-injection, with the exception of persistent cold sensitivity (**Figure 2**). Together, these results suggest that 9-AC induces a transient but reversible increase in the excitability of nociceptive DRG neurons.

Although small- and medium-diameter DRG neurons are the primary mediators of nociception, large-diameter afferents can also contribute to pain signaling under pathological conditions[82-85]. We therefore assessed whether 9-AC affects primary afferents with a large cell body diameter. As shown in **Supplemental Figure 2A**, DRGs were dissociated 6 hours post-injection, and large-diameter neurons were recorded 24 hours later. Representative current-clamp traces showed similar rheobase thresholds between groups (**Supplemental Figure 2B**), and quantification revealed no differences in resting membrane potential or rheobase (**Supplemental Figure 2C-D**), suggesting that large-diameter afferents are not sensitized in this model.

9-AC reduces A-fiber component of the compound action potential

To further evaluate changes in peripheral input, we examined compound action potentials (CAPs) from sciatic nerves *ex vivo*, 24 hours after 9-AC injection. CAPs provide a measure of axonal recruitment and excitability in response to electrical stimulation **(Figure 4A)**. Analysis of C-fiber responses revealed no change in conduction velocity or area under the curve **(**AUC, **Supplemental Figure 3)**, indicating intact unmyelinated fiber function. In contrast, A-fiber responses were significantly impaired following 9-AC treatment. Representative traces showed reduced A-wave amplitudes across a range of stimulation intensities (**Figure 4B**) and while conduction velocity (**Figure 4C**), and activity-dependent suppression of A-fibers at 30 Hz (2.1 ± 0.7 vs 0.6 ± 2.1%) and 100 Hz (14.3 ± 6.9 vs 3.2 ± 3.9%) (vehicle vs 9-AC treated, respectively) remained unchanged, several recruitment metrics were altered. Specifically, 9-AC reduced the AUCMax **(Figure 4D**), shifted the A-wave recruitment curve to the right (**Figure 4E**), which was associated with a significant increase in the current required to reach half-maximal activation (**Figure 4F**), and produced a trend toward a shallower slope in the stimulus-response function (**Figure 4G**). These results indicate that 9-AC reduces the number of functional A-fibers and/or their excitability without producing overt conduction block.

9-AC enhances sensory-evoked activity in the parabrachial nucleus

Peripheral sensory neurons are the first relay in the nociceptive circuit, but central circuits ultimately determine pain perception. To identify central contributors to 9-AC-induced hypersensitivity, we next

bioRxiv preprint doi: https://doi.org/10.1101/2024.06.19.599732; this version posted June 28, 2025. The copyright holder for this preprint (which was not certified by peer review) is the author/funder, who has granted bioRxiv a license to display the preprint in perpetuity. It is made available under aCC-BY-NC 4.0 International license.

investigated the parabrachial nucleus (PBN), a key brainstem structure that integrates spinal nociceptive input and projects to higher-order brain regions involved in affective and motivational aspects of pain[86-88]. We used *in vivo* fiber photometry to monitor calcium activity in glutamatergic PBN neurons in awake, freely moving mice. Mice received stereotaxic injections of an adeno-associated virus encoding GCaMP6s, a genetically encoded calcium sensor that fluoresces in response to intracellular calcium elevations, which serve as a proxy for neuronal activation. The virus was targeted to the PBN to drive selective expression in local glutamatergic neurons. Additionally, an optical fiber cannula was implanted above the injection site to allow repeated recordings from awake, freely behaving animals. After baseline recordings, we re-assessed sensory-evoked PBN activity 24 hours after 9-AC or vehicle administration. After a one-month washout period, animals received the alternate treatment to enable within-subject comparisons (**Figure 5A**).

We observed robust enhancement of sensory-evoked activity in the PBN following 9-AC treatment. Light mechanical stimulation with a 0.07 g von Frey filament elicited exaggerated calcium transients (**Figure 5B-D**), with a significant increase in AUC compared to vehicle (**Figure 5E**). Similar increases were observed with a 1.0 g filament (**Figure 5F-H**), acetone application (**Figure 5J-L**), and pinprick stimulation (**Figure 5N-P**), each showing corresponding AUC increases (**Figure 5I, 5M, 5Q**). These findings indicate that a single episode of myotonia is sufficient to sensitize central pain-processing circuits, supporting a role for central amplification in sustaining nociceptive hypersensitivity.

DM1 mice exhibit persistent pain-like behavior and increased DRG excitability

Although 9-AC mimics an acute myotonic episode similar to that observed in myotonia congenita[21], patients do not experience transient myotonic episodes but rather recurrent myotonia throughout life due to underlying genetic mutations. We therefore hypothesized that mice with myotonia-producing genetic mutations may exhibit persistent pain-like behavior. To test this hypothesis, we used the well characterized HSA LR20b transgenic mouse model of DM1[89]. This genetically engineered mouse model carries a transgene for human skeletal actin (HSA) with an expanded CTG repeat sequence of ~220 repeats in the 3' untranslated region, mimicking the CTG repeat expansion in the *DMPK* gene seen in human DM1[89]. The expression of expanded CTG repeats triggers aberrant splicing of *Clcn1* in skeletal muscle and reduces the surface expression of CLC-1 in muscle fibers producing recurrent myotonia in these mice[16,18] **(Figure 6A)**. Behavioral testing revealed that DM1 mice exhibit significantly reduced withdrawal thresholds to von Frey stimulation **(Figure 6B)**, increased responsiveness to dynamic brushing **(Figure 6C)**, exaggerated responses to acetone application **(Figure 6D)**, and reduced hot plate withdrawal latency **(Figure 6E)**. These results demonstrate that chronic myotonia produces persistent hypersensitivity across sensory modalities.

To assess peripheral mechanisms, we performed *in vitro* whole-cell recordings from sensory neurons with small cell body diameter in adult DM1 and wild-type mice **(Figure 7A)**. Representative traces revealed increased AP firing in DM1 neurons compared to controls **(Figure 7B)**. Quantification showed a significant

bioRxiv preprint doi: https://doi.org/10.1101/2024.06.19.599732; this version posted June 28, 2025. The copyright holder for this preprint (which was not certified by peer review) is the author/funder, who has granted bioRxiv a license to display the preprint in perpetuity. It is made available under aCC-BY-NC 4.0 International license.

depolarization of the resting membrane potential in DM1 neurons **(Figure 7C)**, no change in rheobase **(Figure 7D)**, and a marked increase in the number of evoked APs **(Figure 7E)**, indicating sustained peripheral sensitization in this genetic model. We also examined sensory neurons with a large cell body diameter in DM1 mice **(Supplemental Figure 4A)**. Representative current-clamp traces showed no difference in rheobase between groups **(Supplemental Figure 4B)**, and quantification confirmed no change in resting membrane potential or rheobase **(Supplemental Figure 4C-D)**. These data suggest that myotonia-induced peripheral sensitization is selective for small-diameter nociceptive afferents.

bioRxiv preprint doi: https://doi.org/10.1101/2024.06.19.599732; this version posted June 28, 2025. The copyright holder for this preprint (which was not certified by peer review) is the author/funder, who has granted bioRxiv a license to display the preprint in perpetuity. It is made available under aCC-BY-NC 4.0 International license.

Discussion

This study provides the first experimental evidence that myotonia, independent of overt injury or systemic pathology, is sufficient to evoke persistent increases in the behavioral responses to noxious stimulation in preclinical models, consistent with the pain phenotype described in patients suffering from myotonia. Both pharmacological and genetic induction of muscle hyperexcitability produced robust and prolonged hypersensitivity to mechanical, thermal, and cold stimuli. These behavioral changes were accompanied by increased excitability in putative nociceptive peripheral sensory neurons, a decrease in the excitability of rapidly conducting axons, and amplified activity in central nociceptive circuits. Together, these findings establish a direct mechanistic link between sustained muscle membrane instability and pathological nociceptive processing, offering a novel framework for investigating pain in myotonic disorders.

Mechanistic Insights into Peripheral and Central Sensitization

CLCN1, the gene implicated in producing myotonia in myotonia congenita and DM1, encodes the skeletal muscle chloride channel CLC-1. This channel governs membrane repolarization in myofibers, and its disruption leads to delayed relaxation, repetitive firing, and pathological excitability. Importantly, *Clcn1* is not expressed in primary sensory neurons under either physiological or pathological conditions[90]. This suggests that the channelopathy does not directly alter sensory neuron function. Instead, we hypothesize that pain reported in these patients is due to changes in sensory neurons secondary to the repeated, involuntary contractions and sustained hyperexcitability of the muscle sarcolemma in myotonia (**Figure 8**). Sensory neuron changes are likely due to repetitive mechanical activation of nociceptive free nerve endings that innervate muscle tissue on the one hand, and a compensatory decrease in low threshold muscle afferent (spindles and tendon organs) excitability. The changes in both putative nociceptive and non-nociceptive afferents are likely to contribute to altered CNS processing of noxious stimuli, lowering thresholds for activation and amplifying responses to otherwise innocuous stimuli. This model aligns with established frameworks for both peripheral and central sensitization in chronic pain[91,92].

Consistent with this hypothesis, our *in vitro* electrophysiological recordings reveal increased action potential firing in putative nociceptive sensory neurons, consistent with peripheral sensitization as a key driver of the pain-like behavior observed in our models. At the same time, we observed decreased A-fiber excitability and recruitment, suggesting a loss of low-threshold afferent input that normally maintains segmental inhibition within the spinal cord. According to gate control theory, Aβ fibers exert inhibitory control over spinal nociceptive transmission by activating local spinal inhibitory interneurons[93]. Disruption of this input could remove an important brake, allowing nociceptive signals to dominate and promoting vulnerability to central sensitization[94]. This mechanism offers a compelling explanation for the exaggerated pain-like behavior observed after a single myotonic episode, even in the absence of overt injury (**Figure 8**).

bioRxiv preprint doi: https://doi.org/10.1101/2024.06.19.599732; this version posted June 28, 2025. The copyright holder for this preprint (which was not certified by peer review) is the author/funder, who has granted bioRxiv a license to display the preprint in perpetuity. It is made available under aCC-BY-NC 4.0 International license.

Implication for Nociplastic Pain

These observations fit within the emerging conceptual framework of nociplastic pain, a category proposed by the International Association for the Study of Pain to describe pain arising from altered nociceptive processing in the absence of identifiable tissue or nerve injury[95]. Nociplastic pain presents as multifocal pain accompanied by central nervous system comorbidities such as fatigue, sleep disturbances, and mood disorders. The symptom profile of myotonic disorders and the changes in nociceptive signaling described in the present study are consistent with the definition of nociplastic pain with evidence of augmented peripheral and/or central sensitization in the absence of injury to the nervous system or other evidence of tissue injury or inflammation[96-99]. Myotonic patients frequently report diffuse, treatment-resistant muscle pain, and a significant proportion are misdiagnosed with fibromyalgia or meet its diagnostic criteria[46,48,100,101]. Our findings provide experimental support for the hypothesis that myotonia, through persistent muscle hyperactivity, may drive a form of muscle-originating nociplastic pain via both peripheral and central sensitization.

Future Directions

Future studies should investigate whether similar changes occur in patients with myotonic disorders. Techniques such as microneurography, quantitative sensory testing, and electrically evoked Aβ responses could assess A-fiber integrity and its role in central pain processing. Notably, clinical studies have already identified sensory neuron abnormalities, altered peripheral nerve function, and reduced intraepidermal nerve fiber density in individuals with myotonic dystrophy[52,59,102-105], suggesting that comparable peripheral changes may be at play in the clinical pain phenotype. At the same time, our finding that 9-AC sharply increases calcium activity in the parabrachial nucleus raises the intriguing possibility that central sensitization contributes substantially to the maintenance of myotonia-associated pain. Future studies should directly test this hypothesis by interrogating spinal and supraspinal circuits, including the parabrachial nucleus[87,106], as candidate substrates for nociplastic pain in myotonic disorders. In myotonic patients, functional MRI and other neuroimaging approaches could be used to assess activity across pain-associated brain regions in response to noxious input, providing a translational bridge between preclinical discoveries and clinical observations. Together, such studies will be critical for identifying the central and peripheral mechanisms that sustain nociplastic pain in myotonic disorders.

Although both the 9-AC and DM1 models of myotonia produced increased action potential firing in DRG neurons, indicating peripheral sensitization, only DM1 mice showed a modest but significant depolarization of the resting membrane potential, approximately 4 mV more positive than wild-type controls. This electrophysiological divergence likely reflects the chronic nature of *Clcn1* dysfunction in DM1, in contrast to the transient pharmacological effects of 9-AC. Persistent sarcolemmal hyperexcitability in DM1 may induce secondary changes in sensory neurons over time, possibly through disruption of potassium channel expression or function. Depolarized membrane potentials could result from reduced potassium

bioRxiv preprint doi: https://doi.org/10.1101/2024.06.19.599732; this version posted June 28, 2025. The copyright holder for this preprint (which was not certified by peer review) is the author/funder, who has granted bioRxiv a license to display the preprint in perpetuity. It is made available under aCC-BY-NC 4.0 International license.

conductance, such as diminished activity of leak channels or inward rectifiers[107], but this was not directly tested. Additionally, while both models showed increased firing, the specific ion channels contributing to this hyperexcitability remain undefined. Likely candidates include voltage-gated sodium (Na_V) channels, which play central roles in shaping neuronal firing thresholds and frequency[108]. Future electrophysiological studies using voltage-clamp techniques and pharmacological tools will be essential to dissect the individual channel contributions and fully elucidate the mechanisms driving sensory neuron sensitization in chronic myotonic disease.

Limitations and Conclusions

One limitation of this study is that we simplify the myotonic disorder experience to only CLC-1 blockade/ dysregulation. By contrast, myotonic patients, particularly those with myotonic dystrophies, often present with a range of neurological comorbidities and muscle pathologies that can significantly complicate their pain experience. Despite this complexity, our primary aim was to investigate whether a single or recurrent myotonic episodes could induce pain-like behavior and neuronal pathology. To achieve this, we used the CLC-1 preferring antagonist, 9-AC, and utilized a mouse model of DM1 that primarily mimics muscle pathology while overlooking CTG repeats in other body systems, including the nervous system. We consider this approach a strength of our study as it directly implicates myotonia as a causal factor for pain behavior, a connection not previously established. However, it's essential to acknowledge that future research may reveal differences in peripheral sensory involvement compared to what we observed here, especially when using alternative myotonic models or different experimental designs. In particular, our assessment of pain-like behavior relied exclusively on reflexive behavioral measures, which may be influenced by the muscle rigidity and slower movements characteristic of myotonia. In this context, our data might underestimate the perceptual changes associated with myotonia, as rigidity could mask or reduce the expression of behavioral responses. Additionally, our evaluation of pain-like behavior only after a single injection of 9-AC may miss additional mechanisms that develop over time and consequently would only be detected with repeated injections. We also did not explore the relationship between muscle fiber pathology and pain-like behavior. Different sensory pathologies might correspond with specific muscle dysregulations or fiber types. Notably, another murine model of DM1 myotonia has shown transitions between glycolytic and oxidative fiber types[109] and such a transition may affect pain pathophysiology. Lastly, some patients experience painful myotonia due to *SCN4A* mutations rather than *CLCN1*, and this variant of myotonia was not addressed in our preclinical study. In sum, while our findings offer important mechanistic insights, these limitations highlight the need for further work to fully capture the complexities of pain in myotonic disorders.

In conclusion, this work challenges the long-standing assumption that myotonia is a purely motor disorder and establishes a physiological link between muscle hyperexcitability and chronic pain. Our findings indicate that this pain-like behavior is driven by peripheral sensitization and suggests that central mechanisms might be involved too. While we focused on CLC-1 dysregulation, future research should

bioRxiv preprint doi: https://doi.org/10.1101/2024.06.19.599732; this version posted June 28, 2025. The copyright holder for this preprint (which was not certified by peer review) is the author/funder, who has granted bioRxiv a license to display the preprint in perpetuity. It is made available under aCC-BY-NC 4.0 International license.

explore other genetic mutations and the relationship between muscle pathology and pain. These results open new avenues for understanding pain mechanisms in myotonic disorders and developing effective treatments, addressing a significant unmet need in pain management for these conditions.

bioRxiv preprint doi: https://doi.org/10.1101/2024.06.19.599732; this version posted June 28, 2025. The copyright holder for this preprint (which was not certified by peer review) is the author/funder, who has granted bioRxiv a license to display the preprint in perpetuity. It is made available under aCC-BY-NC 4.0 International license.

Acknowledgements

This work was supported was supported by National Institutes of Health (NIH) awards K00NS124190 (to TSN), F32NS128392 (to HNA), K99NS134965 (to KG), and RF1NS131165, R61NS126026, R01NS120663 (to RK). Additionally, this work was supported by a Development Grant from the American Neuromuscular Foundation (to TSN) and a PhRMA Foundation Postdoctoral Fellowship (No. 1335819 to EJRP).

bioRxiv preprint doi: https://doi.org/10.1101/2024.06.19.599732; this version posted June 28, 2025. The copyright holder for this preprint (which was not certified by peer review) is the author/funder, who has granted bioRxiv a license to display the preprint in perpetuity. It is made available under aCC-BY-NC 4.0 International license.

References

1. Heatwole CR, Statland JM, Logigian EL. The diagnosis and treatment of myotonic disorders. *Muscle Nerve*. 2013;47(5):632-648. doi:10.1002/mus.23683
2. Trivedi JR. Muscle Channelopathies. *Contin Lifelong Learn Neurol*. 2022;28(6):1778-1799. doi:10.1212/CON.0000000000001183
3. Stunnenberg BC, LoRusso S, Arnold WD, et al. Guidelines on clinical presentation and management of nondystrophic myotonias. *Muscle and Nerve*. 2020;62(4):430-444. doi:10.1002/mus.26887
4. Hudson AJ, Ebers GC, Bulman DE. The skeletal muscle sodium and chloride channel diseases. *Brain*. 1995;118(2):547-563. doi:10.1093/brain/118.2.547
5. Matthews E, Fialho D, Tan S V., et al. The non-dystrophic myotonias: Molecular pathogenesis, diagnosis and treatment. *Brain*. 2010;133(1):9-22. doi:10.1093/brain/awp294
6. Miller TM. Differential diagnosis of myotonic disorders. *Muscle Nerve*. 2008;37(3):293-299. doi:10.1002/mus.20923
7. Sansone VA, Ricci C, Montanari M, Apolone G, Rose M, Meola G. Measuring quality of life impairment in skeletal muscle channelopathies. *Eur J Neurol*. 2012;19(11):1470-1476. doi:10.1111/j.1468-1331.2012.03751.x
8. Trivedi JR, Bundy B, Statland J, et al. Non-dystrophic myotonia: Prospective study of objective and patient reported outcomes. *Brain*. 2013;136(7):2189-2200. doi:10.1093/brain/awt133
9. Matthews E, Holmes S, Fialho D. Skeletal muscle channelopathies: A guide to diagnosis and management. *Pract Neurol*. 2021;21(3):196-205. doi:10.1136/practneurol-2020-002576
10. Pedersen TH, Riisager A, de Paoli FV, Chen TY, Nielsen OB. Role of physiological ClC-1 Cl- ion channel regulation for the excitability and function of working skeletal muscle. *J Gen Physiol*. 2016;147(4):291-308. doi:10.1085/jgp.201611582
11. Tang C-Y, Chen T-Y. Physiology and Pathophysiology of CLC-1: Mechanisms of a Chloride Channel Disease, Myotonia. *J Biomed Biotechnol*. 2011;2011:1-10. doi:10.1155/2011/685328
12. Koch MC, Steinmeyer K, Lorenz C, et al. The Skeletal Muscle Chloride Channel in Dominant and Recessive Human Myotonia. *Science (80-)*. 1992;257(5071):797-800. doi:10.1126/science.1379744
13. Zhang J, George AL, Griggs RC, et al. Mutations in the human skeletal muscle chloride channel gene (CLCN1) associated with dominant and recessive myotonia congenita. *Neurology*. 1996;47(4):993-998. doi:10.1212/WNL.47.4.993
14. Plassart-Schiess E, Gervais A, Eymard B, et al. Novel muscle chloride channel (CLCN1) mutations in myotonia congenita with various modes of inheritance including incomplete dominance and penetrance. *Neurology*. 1998;50(4):1176-1179. doi:10.1212/WNL.50.4.1176
15. Steinmeyer K, Klocke R, Ortland C, et al. Inactivation of muscle chloride channel by transposon

bioRxiv preprint doi: https://doi.org/10.1101/2024.06.19.599732; this version posted June 28, 2025. The copyright holder for this preprint (which was not certified by peer review) is the author/funder, who has granted bioRxiv a license to display the preprint in perpetuity. It is made available under aCC-BY-NC 4.0 International license.

insertion in myotonic mice. *Nature*. 1991;354(6351):304-308. doi:10.1038/354304a0

16. Mankodi A, Takahashi MP, Jiang H, et al. Expanded CUG repeats trigger aberrant splicing of ClC-1 chloride channel pre-mRNA and hyperexcitability of skeletal muscle in myotonic dystrophy. *Mol Cell*. 2002;10(1):35-44. doi:10.1016/S1097-2765(02)00563-4
17. Lueck JD, Lungu C, Mankodi A, et al. Chloride channelopathy in myotonic dystrophy resulting from loss of posttranscriptional regulation for CLCN1. *Am J Physiol - Cell Physiol*. 2007;292(4):1291-1297. doi:10.1152/ajpcell.00336.2006
18. Charlet-B N, Savkur RS, Singh G, Philips A V, Grice EA, Cooper TA. Loss of the Muscle-Specific Chloride Channel in Type 1 Myotonic Dystrophy Due to Misregulated Alternative Splicing several lines of evidence indicate that a gain of function for RNA CUG)n. *Mol Cell*. 2002;10:45-53.
19. Pohl J, Hesse E. Zur Pharmakologie des Tetrophans. *Klin Wochenschr*. 1925;4(8):343-344. doi:10.1007/BF01745254
20. Bretag AH, Dawe SR, Moskwa AG. Chemically induced myotonia in amphibia. *Nature*. 1980;286(5773):625-626. doi:10.1038/286625a0
21. Bryant SH, Morales-Aguilera A. Chloride conductance in normal and myotonic muscle fibres and the action of monocarboxylic aromatic acids. *J Physiol*. 1971;219(2):367-383. doi:10.1113/jphysiol.1971.sp009667
22. Furman RE, Barchi RL. The pathophysiology of myotonia produced by aromatic carboxylic acids. *Ann Neurol*. 1978;4(4):357-365. doi:10.1002/ana.410040411
23. Eddy NB. Studies of Phenanthrene Derivatives I. A Comparison of Phenanthrene 2-, 3-, and 9-Monosubstitution Products. *J Pharmacol Exp Ther*. 1933;48(2):183-198.
24. Smith GR. Studies of Phenanthrene Derivatives Iv. a Veratrine-Like Action on Skeletal Muscle of Certain 9-Substitution Products of Phenanthrene. *J Pharmacol Exp Ther*. 1935;54(1):87-99. https://physoc.onlinelibrary.wiley.com/doi/10.1113/jphysiol.1971.sp009667.
25. Kwieciński H, Barchi RL. Myotonia Induced by Chemical Agents. *CRC Crit Rev Toxicol*. 1981;8(4):279-310. doi:10.3109/10408448109089901
26. Palade PT, Barchi RL. On the inhibition of muscle membrane chloride conductance by aromatic carboxylic acids. *J Gen Physiol*. 1977;69(6):879-896. doi:10.1085/jgp.69.6.879
27. Brody IA. Myotonia Induced by Monocarboxylic Aromatic Acids. *Arch Neurol*. 1973;28(4):243. doi:10.1001/archneur.1973.00490220051007
28. Estévez R, Schroeder BC, Accardi A, Jentsch TJ, Pusch M. Conservation of chloride channel structure revealed by an inhibitor binding site in ClC-1. *Neuron*. 2003;38(1):47-59. doi:10.1016/S0896-6273(03)00168-5
29. Altamura C, Mangiatordi GF, Nicolotti O, et al. Mapping ligand binding pockets in chloride ClC-1 channels through an integrated in silico and experimental approach using anthracene-9-carboxylic acid and niflumic acid. *Br J Pharmacol*. 2018;175(10):1770-1780. doi:10.1111/bph.14192
30. Villegas-Navarro A, Martinez-Morales M, Morales-Aguilera A. Pharmacokinetics of anthracene-9-

bioRxiv preprint doi: https://doi.org/10.1101/2024.06.19.599732; this version posted June 28, 2025. The copyright holder for this preprint (which was not certified by peer review) is the author/funder, who has granted bioRxiv a license to display the preprint in perpetuity. It is made available under aCC-BY-NC 4.0 International license.

carboxylic acid, a potent myotonia-inducer. *Arch Int Pharmacodyn Ther*. 1986;280(1):5-21.

31. Desaphy JF, Costanza T, Carbonara R, Conte Camerino D. In vivo evaluation of antimyotonic efficacy of β-adrenergic drugs in a rat model of myotonia. *Neuropharmacology*. 2013;65:21-27. doi:10.1016/j.neuropharm.2012.09.006
32. Desaphy JF, Carbonara R, Costanza T, Conte Camerino D. Preclinical evaluation of marketed sodium channel blockers in a rat model of myotonia discloses promising antimyotonic drugs. *Exp Neurol*. 2014;255:96-102. doi:10.1016/j.expneurol.2014.02.023
33. Camerino DC, De Luca A, Mambrini M, et al. The effects of taurine on pharmacologically induced myotonia. *Muscle Nerve*. 1989;12(11):898-904. doi:10.1002/mus.880121105
34. Mrozek K, Kaminska A, Kwiecinski H. Experimental myotonia myotonic activity of the fast and slow muscles. *Acta Physiol Pol*. 1974;25(4):321-327.
35. Welsh MJ. Anthracene-9-carboxylic acid inhibits an apical membrane, chloride conductance in canine tracheal epithelium. *J Membr Biol*. 1984;78(1):61-71. doi:10.1007/BF01872533
36. Bandschapp O, Ginz HF, Soule CL, Girard T, Urwyler A, Iaizzo PA. In Vitro Effects of Propofol and Volatile Agents on Pharmacologically Induced Chloride Channel Myotonia. *Anesthesiology*. 2009;111(3):584-590. doi:10.1097/ALN.0b013e3181b05f23
37. Kwiecińaski H, Lehmann-Horn F, Rüdel R. Drug-induced myotonia in human intercostal muscle. *Muscle Nerve*. 1988;11(6):576-581. doi:10.1002/mus.880110609
38. Hoppe K, Sartorius T, Chaiklieng S, et al. Paxilline Prevents the Onset of Myotonic Stiffness in Pharmacologically Induced Myotonia: A Preclinical Investigation. *Front Physiol*. 2020;11(November). doi:10.3389/fphys.2020.533946
39. Sethi PD. Antagonism of anthracene 9 carboxylic acid as screening test for muscle relaxants. *Indian J Physiol Pharmacol*. 1976;20(4):239-241.
40. Desaphy JF, Farinato A, Altamura C, et al. Safinamide's potential in treating nondystrophic myotonias: Inhibition of skeletal muscle voltage-gated sodium channels and skeletal muscle hyperexcitability in vitro and in vivo. *Exp Neurol*. 2020;328(March):113287. doi:10.1016/j.expneurol.2020.113287
41. De Bellis M, Carbonara R, Roussel J, et al. Increased sodium channel use-dependent inhibition by a new potent analogue of tocainide greatly enhances in vivo antimyotonic activity. *Neuropharmacology*. 2017;113:206-216. doi:10.1016/j.neuropharm.2016.10.013
42. White WH. On some recent advances in our knowledge of thomsen's disease. *Brain*. 1886;9(1):112-119. doi:10.1093/brain/9.1.112
43. Dana CL. An Atypical Case of Thomsen's Disease (Myotonia Congenita). *Med Rec*. 1888;33(16):433. doi:info:doi/
44. Deligny L. Observation d'un cas de maladie de Thommsen. *L'UNION MÉDICALE*. 1885;XXXIX(1):50-52.
45. Wood HC. *Nervous Diseases and Their Diagnosis: A Treatise upon the Phenomena Produced by*

bioRxiv preprint doi: https://doi.org/10.1101/2024.06.19.599732; this version posted June 28, 2025. The copyright holder for this preprint (which was not certified by peer review) is the author/funder, who has granted bioRxiv a license to display the preprint in perpetuity. It is made available under aCC-BY-NC 4.0 International license.

Diseases of the Nervous System, with Especial Reference to the Recognition of Their Causes. Vol 33. Philadelphia: J. B. Lippincott company; 1887. doi:10.1192/bjp.33.143.431

46. Giacobbe A, Subramony S, Chuquilin M. Pain as a significant symptom in patients with periodic paralysis—A cross-sectional survey. *Muscle and Nerve*. 2021;63(6):897-901. doi:10.1002/mus.27241
47. Trip J, De Vries J, Drost G, Ginjaar HB, van Engelen BGMM, Faber CG. Health status in non-dystrophic myotonias: close relation with pain and fatigue. *J Neurol*. 2009;256(6):939-947. doi:10.1007/s00415-009-5049-y
48. Nam TS, Choi SY, Park DJ, Lee SS, Kim YO, Kim MK. The overlap between fibromyalgia syndrome and myotonia congenita. *J Clin Neurol*. 2015;11(2):188-191. doi:10.3988/jcn.2015.11.2.188
49. Sanders DB. Myotonia Congenita With Painful Muscle Contractions. *Arch Neurol*. 1976;33(8):580-582. doi:10.1001/archneur.1976.00500080058009
50. Sunohara N, Tomi H, Nakamura A, Arahata K, Nonaka I. Myotonia congenita with painful muscle cramps. *Intern Med*. 1996;35(6):507-511. doi:10.2169/internalmedicine.35.507
51. Orsini C, Petillo R, D'Ambrosio P, et al. CLCN1 Molecular Characterization in 19 South-Italian Patients With Dominant and Recessive Type of Myotonia Congenita. *Front Neurol*. 2020;11(February):1-6. doi:10.3389/fneur.2020.00063
52. Moshourab R, Palada V, Grunwald S, Grieben U, Lewin GR, Spuler S. A Molecular Signature of Myalgia in Myotonic Dystrophy 2. *EBioMedicine*. 2016;7:205-211. doi:10.1016/j.ebiom.2016.03.017
53. Parmova O. The Character and Frequency of Muscular Pain in Myotonic Dystrophy and Their Relationship to Myotonia. *Int J Neurol Neurother*. 2014;1(1):1-5. doi:10.23937/2378-3001/1/1/1009
54. Peric M, Peric S, Rapajic N, et al. Multidimensional aspects of pain in myotonic dystrophies. *Acta Myol myopathies cardiomyopathies Off J Mediterr Soc Myol*. 2015;34(2-3):126-132.
55. Jensen MP, Hoffman AJ, Stoelb BL, Abresch RT, Carter GT, McDonald CM. Chronic Pain in Persons With Myotonic Dystrophy and Facioscapulohumeral Dystrophy. *Arch Phys Med Rehabil*. 2008;89(2):320-328. doi:10.1016/j.apmr.2007.08.153
56. Miró J, Gertz KJ, Carter GT, Jensen MP. Pain location and intensity impacts function in persons with myotonic dystrophy type 1 and facioscapulohumeral dystrophy with chronic pain. *Muscle and Nerve*. 2014;49(6):900-905. doi:10.1002/mus.24079
57. Solbakken G, Løseth S, Froholdt A, et al. Pain in adult myotonic dystrophy type 1: relation to function and gender. *BMC Neurol*. 2021;21(1):1-11. doi:10.1186/s12883-021-02124-9
58. Liguori S, Moretti A, Toro G, et al. Pain and Motor Function in Myotonic Dystrophy Type 1: A Cross-Sectional Study. *Int J Environ Res Public Health*. 2023;20(7):1-11. doi:10.3390/ijerph20075244
59. van Vliet J, Tieleman AA, Verrips A, et al. Qualitative and Quantitative Aspects of Pain in Patients

bioRxiv preprint doi: https://doi.org/10.1101/2024.06.19.599732; this version posted June 28, 2025. The copyright holder for this preprint (which was not certified by peer review) is the author/funder, who has granted bioRxiv a license to display the preprint in perpetuity. It is made available under aCC-BY-NC 4.0 International license.

With Myotonic Dystrophy Type 2. *J Pain*. 2018;19(8):920-930. doi:10.1016/j.jpain.2018.03.006

60. Suokas K, Palmio J, Sandell S, Udd B, Hietaharju A. Pain in SCN4A Mutated P.A1156T muscle sodium channelopathy—a postal survey. *Muscle and Nerve*. 2018;57(6):1014-1017. doi:10.1002/mus.26050
61. Palmio J, Sandell S, Hanna MG, Männikkö R, Penttilä S, Udd B. Predominantly myalgic phenotype caused by the c.3466G>A p.A1156T mutation in SCN4A gene. *Neurology*. 2017;88(16):1520-1527. doi:10.1212/WNL.0000000000003846
62. Bissay V, Keymolen K, Lissens W, Laureys G, Schmedding E, Keyser J De. Late onset painful cold-aggravated myotonia: Three families with SCN4A L1436P mutation. *Neuromuscul Disord*. 2011;21(8):590-593. doi:10.1016/j.nmd.2011.05.006
63. Torbergsen T, Jurkat-Rott K, Stålberg E V., Løseth S, Hødneø A, Lehmann-Horn F. Painful cramps and giant myotonic discharges in a family with the Nav1.4-G1306A mutation. *Muscle and Nerve*. 2015;52(4):680-683. doi:10.1002/mus.24672
64. Periviita V, Männikkö R, Jokela M, et al. Novel SCN4A Variants Associated With Myalgic Myotonic Disorder or Paramyotonia. *Eur J Neurol*. 2025;32(5):e70157. doi:10.1111/ene.70157
65. Rosenfeld J, Sloan-Brown K, George AL. A novel muscle sodium channel mutation causes painful congenital myotonia. *Ann Neurol*. 1997;42(5):811-814. doi:10.1002/ana.410420520
66. Meyer AP, Roggenbuck J, LoRusso S, et al. Genotype-Phenotype Correlations and Characterization of Medication Use in Inherited Myotonic Disorders. *Front Neurol*. 2020;11(June):593. doi:10.3389/fneur.2020.00593
67. Vicart S, Péréon Y, Ghorab K, et al. Self-reported outcomes and quality of life of patients with non-dystrophic myotonia: The French IMPACT 2022 survey. *Rev Neurol (Paris)*. 2024;0:0-6. doi:10.1016/j.neurol.2024.04.007
68. Sagerer E, Wirner-Piotrowski C, Mijic M, et al. Nociceptive Pain in Patients with Neuromuscular Disorders: A Cross-Sectional Clinical Study. *J Neuromuscul Dis*. 2024;11(5):1111-1122. doi:10.3233/JND-240068
69. Schmitt V, Baeumler P, Schänzer A, Irnich D, Schoser B, Montagnese F. Characterization of the neuropathic pain component contributing to myalgia in patients with myotonic dystrophy type 1 and 2. *Front Neurol*. 2024;15(August):1-17. doi:10.3389/fneur.2024.1414140
70. Gomez K, Santiago U, Nelson TS, et al. A peptidomimetic modulator of the CaV2.2 N-type calcium channel for chronic pain. *Proc Natl Acad Sci*. 2023;120(47):e2305215120. doi:10.1073/pnas.2305215120
71. Gomez K, Allen HN, Duran P, et al. Targeted transcriptional upregulation of SENP1 by CRISPR activation enhances deSUMOylation pathways to elicit antinociception in the spinal nerve ligation model of neuropathic pain. *Pain*. 2024;165(4):866-883. doi:10.1097/j.pain.0000000000003080
72. Hestehave S, Allen HN, Gomez K, et al. Small molecule targeting NaV1.7 via inhibition of CRMP2-Ubc9 interaction reduces pain-related outcomes in a rodent osteoarthritic model. *Pain*.

bioRxiv preprint doi: https://doi.org/10.1101/2024.06.19.599732; this version posted June 28, 2025. The copyright holder for this preprint (which was not certified by peer review) is the author/funder, who has granted bioRxiv a license to display the preprint in perpetuity. It is made available under aCC-BY-NC 4.0 International license.

2025;166(1):99-111. doi:10.1097/j.pain.0000000000003357

73. Tang C, Gomez K, Chen Y, et al. C2230, a preferential use- and state-dependent CaV2.2 channel blocker, mitigates pain behaviors across multiple pain models. *J Clin Invest*. 2025;135(4). doi:10.1172/JCI177429
74. Allen HN, Hestehave S, Duran P, Nelson TS, Khanna R. Uncoupling the CRMP2-CaV2.2 Interaction Reduces Pain-Like Behavior in a Preclinical Joint-Pain Model. *J Pain*. 2024;25(12):104664. doi:10.1016/j.jpain.2024.104664
75. Nelson TS, Santos DFS, Prasoon P, Gralinski M, Allen HN, Taylor BK. Endogenous μ-opioid—Neuropeptide Y Y1 receptor synergy silences chronic postoperative pain in mice. Abramov A, ed. *PNAS Nexus*. 2023;2(8):1-11. doi:10.1093/pnasnexus/pgad261
76. Nelson TS, Sinha GP, Santos DFS, et al. Spinal neuropeptide Y Y1 receptor-expressing neurons are a pharmacotherapeutic target for the alleviation of neuropathic pain. *Proc Natl Acad Sci*. 2022;119(46):e2204515119. doi:10.1073/pnas.2204515119
77. Chaplan SR, Bach FW, Pogrel JW, Chung JM, Yaksh TL. Quantitative assessment of tactile allodynia in the rat paw. *J Neurosci Methods*. 1994;53(1):55-63. doi:10.1016/0165-0270(94)90144-9
78. Nelson TS, Fu W, Donahue RR, et al. Facilitation of neuropathic pain by the NPY Y1 receptor-expressing subpopulation of excitatory interneurons in the dorsal horn. *Sci Rep*. 2019;9(1):7248. doi:10.1038/s41598-019-43493-z
79. Qi Y, Nelson TS, Prasoon P, Norris C, Taylor BK. Contribution of μ Opioid Receptor-expressing Dorsal Horn Interneurons to Neuropathic Pain-like Behavior in Mice. *Anesthesiology*. 2023;139(6):840-857. doi:10.1097/ALN.0000000000004735
80. Gold MS, Gebhart GF. Nociceptor sensitization in pain pathogenesis. *Nat Med*. 2010;16(11):1248-1257. doi:10.1038/nm.2235
81. Kuner R. Central mechanisms of pathological pain. *Nat Med*. 2010;16(11):1258-1266. doi:10.1038/nm.2231
82. Sun W, Yang F, Wang Y, et al. Contribution of large-sized primary sensory neuronal sensitization to mechanical allodynia by upregulation of hyperpolarization-activated cyclic nucleotide gated channels via cyclooxygenase 1 cascade. *Neuropharmacology*. 2017;113:217-230. doi:10.1016/j.neuropharm.2016.10.012
83. François A, Schüetter N, Laffray S, et al. The Low-Threshold Calcium Channel Cav3.2 Determines Low-Threshold Mechanoreceptor Function. *Cell Rep*. 2015;10(3):370-382. doi:10.1016/j.celrep.2014.12.042
84. Song Y, Li HM, Xie RG, et al. Evoked bursting in injured Aβ dorsal root ganglion neurons: A mechanism underlying tactile allodynia. *Pain*. 2012;153(3):657-665. doi:10.1016/j.pain.2011.11.030
85. Zhu YF, Henry JL. Excitability of Aβ sensory neurons is altered in an animal model of peripheral

bioRxiv preprint doi: https://doi.org/10.1101/2024.06.19.599732; this version posted June 28, 2025. The copyright holder for this preprint (which was not certified by peer review) is the author/funder, who has granted bioRxiv a license to display the preprint in perpetuity. It is made available under aCC-BY-NC 4.0 International license.

neuropathy. *BMC Neurosci*. 2012;13(1). doi:10.1186/1471-2202-13-15

86. Bernard JF, Besson JM. The spino(trigemino)pontoamygdaloid pathway: Electrophysiological evidence for an involvement in pain processes. *J Neurophysiol*. 1990;63(3):473-490. doi:10.1152/jn.1990.63.3.473
87. Nelson TS, Allen HN. The spino-parabrachio-amygdaloid pathway is critical for the manifestation of chronic pain. *Neuropsychopharmacology*. 2024;49(3):491-492. doi:10.1038/s41386-023-01745-7
88. Palmiter RD. Parabrachial neurons promote nociplastic pain. *Trends Neurosci*. 2024;47(9):722-735. doi:10.1016/j.tins.2024.07.002
89. Mankodi A, Logigian E, Callahan L, et al. Myotonic dystrophy in transgenic mice expressing an expanded CUG repeat. *Science (80-)*. 2000;289(5485):1769-1772. doi:10.1126/science.289.5485.1769
90. Renthal W, Tochitsky I, Yang L, et al. Transcriptional Reprogramming of Distinct Peripheral Sensory Neuron Subtypes after Axonal Injury. *Neuron*. 2020;108(1):128-144.e9. doi:10.1016/j.neuron.2020.07.026
91. Gangadharan V, Kuner R. Pain hypersensitivity mechanisms at a glance. *DMM Dis Model Mech*. 2013;6(4):889-895. doi:10.1242/dmm.011502
92. Latremoliere A, Woolf CJ. Central Sensitization: A Generator of Pain Hypersensitivity by Central Neural Plasticity. *J Pain*. 2009;10(9):895-926. doi:10.1016/j.jpain.2009.06.012
93. Melzack R, Wall PD. Pain mechanisms: A new theory. *Science (80-)*. 1965;150(3699):971-979. doi:10.1126/science.150.3699.971
94. Guo D, Hu J. Spinal presynaptic inhibition in pain control. *Neuroscience*. 2014;283:95-106. doi:10.1016/j.neuroscience.2014.09.032
95. Kosek E, Cohen M, Baron R, et al. Do we need a third mechanistic descriptor for chronic pain states? *Pain*. 2016;157(7):1382-1386. doi:10.1097/j.pain.0000000000000507
96. Kaplan CM, Kelleher E, Irani A, Schrepf A, Clauw DJ, Harte SE. Deciphering nociplastic pain: clinical features, risk factors and potential mechanisms. *Nat Rev Neurol*. 2024;20(6):347-363. doi:10.1038/s41582-024-00966-8
97. Fitzcharles MA, Cohen SP, Clauw DJ, Littlejohn G, Usui C, Häuser W. Nociplastic pain: towards an understanding of prevalent pain conditions. *Lancet*. 2021;397(10289):2098-2110. doi:10.1016/S0140-6736(21)00392-5
98. Yoo YM, Kim KH. Current understanding of nociplastic pain. *Korean J Pain*. 2024;37(2):107-118. doi:10.3344/kjp.23326
99. Kosek E. The concept of nociplastic pain—where to from here? *Pain*. 2024;165(11S):S50-S57. doi:10.1097/j.pain.0000000000003305
100. Auvinen S, Suominen T, Hannonen P, Bachinski LL, Krahe R, Udd B. Myotonic dystrophy type 2 found in two of sixty-three persons diagnosed as having fibromyalgia. *Arthritis Rheum*.

bioRxiv preprint doi: https://doi.org/10.1101/2024.06.19.599732; this version posted June 28, 2025. The copyright holder for this preprint (which was not certified by peer review) is the author/funder, who has granted bioRxiv a license to display the preprint in perpetuity. It is made available under aCC-BY-NC 4.0 International license.

2008;58(11):3627-3631. doi:10.1002/art.24037

101. Götze FR, Thid S, Kyllerman M. Fibromyalgia in hyperkalemic periodic paralysis. *Scand J Rheumatol*. 1998;27(5):383-384. doi:10.1080/03009749850154456
102. George A, Schneider-Gold C, Zier S, Reiners K, Sommer C. Musculoskeletal pain in patients with myotonic dystrophy type 2. *Arch Neurol*. 2004;61(12):1938-1942. doi:10.1001/archneur.61.12.1938
103. Boland-Freitas R, Ng K. Assessment of small sensory fiber function in myotonic dystrophy type 1. *Muscle Nerve*. 2019;60(5):575-579. doi:10.1002/mus.26673
104. Solbakken G, Løseth S, Frich JC, Dietrichs E, Ørstavik K. Small and large fiber neuropathy in adults with myotonic dystrophy type 1. *Front Neurol*. 2024;15(March):1-5. doi:10.3389/fneur.2024.1375218
105. Hermans MCE, Faber CG, Vanhoutte EK, et al. Peripheral neuropathy in myotonic dystrophy type 1. *J Peripher Nerv Syst*. 2011;16(1):24-29. doi:10.1111/j.1529-8027.2011.00313.x
106. Condon LF, Yu Y, Park S, et al. Parabrachial Calca neurons drive nociplasticity. *Cell Rep*. 2024;43(4):114057. doi:10.1016/j.celrep.2024.114057
107. Xiao Y, Wu Y, Zhao B, Xia Z. Decreased voltage-gated potassium currents in rat dorsal root ganglion neurons after chronic constriction injury. *Neuroreport*. 2016;27(2):104-109. doi:10.1097/WNR.0000000000000505
108. Bennett DL, Clark XAJ, Huang J, Waxman SG, Dib-Hajj SD. The role of voltage-gated sodium channels in pain signaling. *Physiol Rev*. 2019;99(2):1079-1151. doi:10.1152/physrev.00052.2017
109. Hu N, Kim E, Antoury L, Wheeler TM. Correction of Clcn1 alternative splicing reverses muscle fiber type transition in mice with myotonic dystrophy. *Nat Commun*. 2023;14(1). doi:10.1038/s41467-023-37619-1

bioRxiv preprint doi: https://doi.org/10.1101/2024.06.19.599732; this version posted June 28, 2025. The copyright holder for this preprint (which was not certified by peer review) is the author/funder, who has granted bioRxiv a license to display the preprint in perpetuity. It is made available under aCC-BY-NC 4.0 International license.

Figures

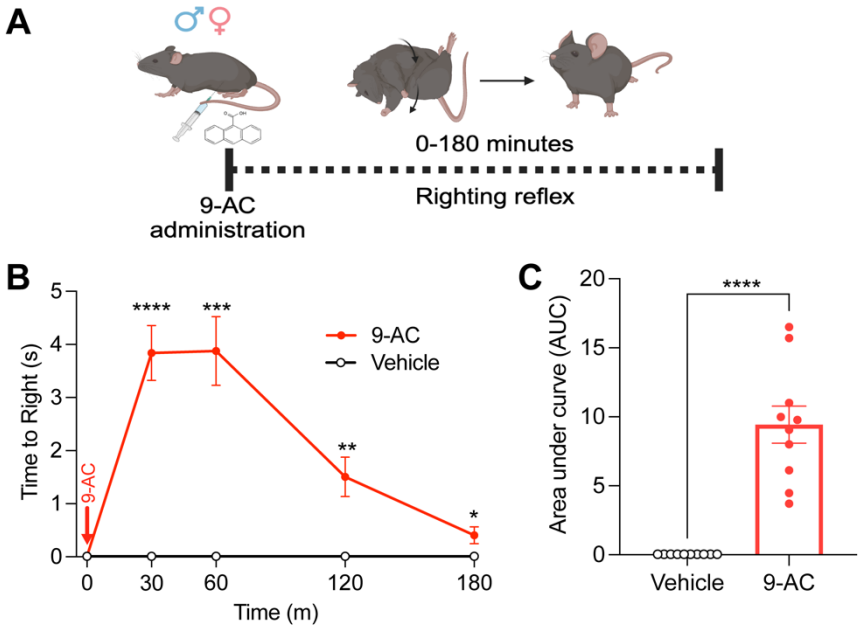

Figure 1. Anthracene-9-carboxylic acid (9-AC) induces transient myotonic behavior in mice. (A) Schematic illustrating the experimental timeline. Mice received a single intraperitoneal injection of 9-AC (30 mg/kg), followed by measurement of the righting reflex to assess myotonia-like muscle stiffness *in vivo*. **(B)** Time course of righting reflex latency analyzed by two-way repeated-measures ANOVA followed by Holm-Sidak's post hoc test. **(C)** Quantification of area under the curve (AUC) analyzed by unpaired two-tailed Student's t test. Data are presented as mean ± SEM (n = 10 mice/group). Individual data points represent values from individual animals. *$p < 0.05$, **$p < 0.01$, ***$p < 0.001$, ****$p < 0.0001$. In some instances, error bars are too small to be visually discernible.

bioRxiv preprint doi: https://doi.org/10.1101/2024.06.19.599732; this version posted June 28, 2025. The copyright holder for this preprint (which was not certified by peer review) is the author/funder, who has granted bioRxiv a license to display the preprint in perpetuity. It is made available under aCC-BY-NC 4.0 International license.

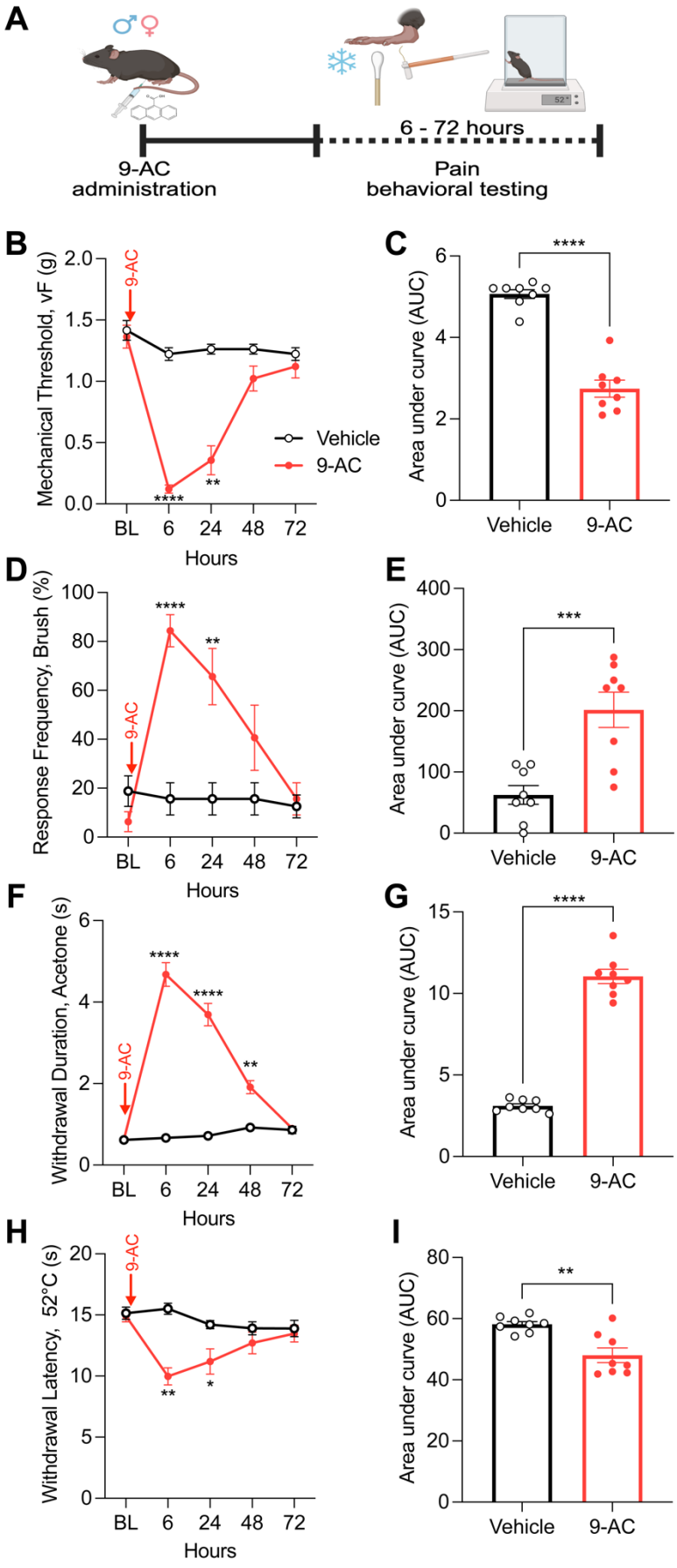

bioRxiv preprint doi: https://doi.org/10.1101/2024.06.19.599732; this version posted June 28, 2025. The copyright holder for this preprint (which was not certified by peer review) is the author/funder, who has granted bioRxiv a license to display the preprint in perpetuity. It is made available under aCC-BY-NC 4.0 International license.

Figure 2. Pharmacological induction of myotonia with 9-AC induces persistent pain-like behavior in mice. (A) Schematic of the experimental timeline showing intraperitoneal administration of 9-AC (30 mg/kg) followed by behavioral pain testing over a 72-hour period. **(B-C)** Static mechanical allodynia assessed using von Frey filaments. **(D-E)** Dynamic mechanical allodynia assessed using brush stimulation. **(F-G)** Cold allodynia assessed via acetone droplet application. **(H-I)** Thermal hyperalgesia measured using a 52 °C hot plate assay. **(B, D, F, H)** Time course data were analyzed using two-way ANOVA followed by Sidak's post hoc test. **(C, E, G, I)** Area under the curve (AUC) values were analyzed using unpaired two-tailed Student's t test. Data are presented as mean ± SEM (n = 8 mice/group). Individual data points represent values from individual animals. *$p < 0.05$, **$p < 0.01$, ***$p < 0.001$, ****$p < 0.0001$. In some instances, error bars are too small to be visually discernible.

bioRxiv preprint doi: https://doi.org/10.1101/2024.06.19.599732; this version posted June 28, 2025. The copyright holder for this preprint (which was not certified by peer review) is the author/funder, who has granted bioRxiv a license to display the preprint in perpetuity. It is made available under aCC-BY-NC 4.0 International license.

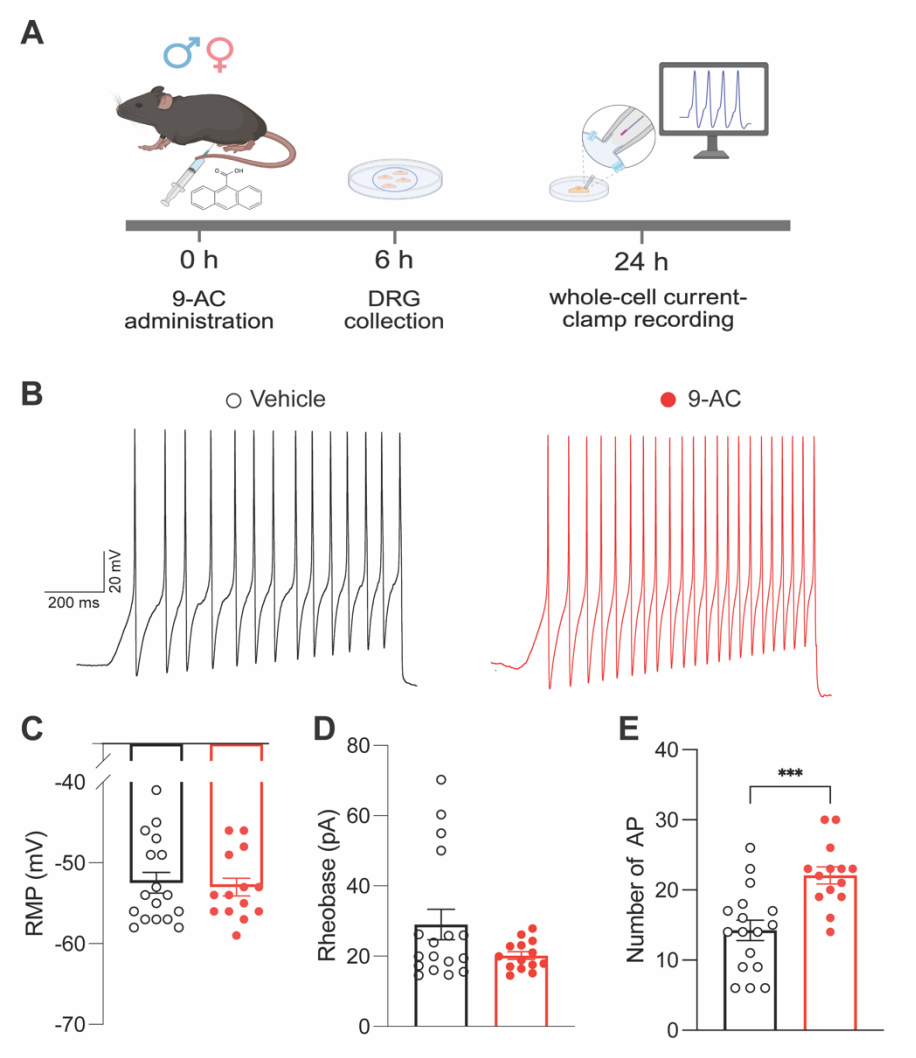

Figure 3. 9-AC increases the excitability of dorsal root ganglion neurons. (A) Schematic illustrating the experimental timeline. Mice received a single intraperitoneal injection of 9-AC (30 mg/kg), followed by lumbar DRG dissociation 6 hours later. Whole-cell current-clamp recordings were performed in small- and medium-diameter DRG neurons 24 hours post-injection. **(B)** Representative traces showing action potential (AP) firing in sensory neurons from vehicle-treated (left) and 9-AC-treated (right) animals in response to suprathreshold current injection. **(C-E)** Quantification of (**C**) resting membrane potential (RMP), (**D**) rheobase, and (**E**) number of evoked APs. Data were analyzed using the Mann-Whitney U test. Data are presented as mean ± SEM (n = 15-17 neurons from 4 mice/group). Individual data points represent values from single neurons. ***$p < 0.001$.

bioRxiv preprint doi: https://doi.org/10.1101/2024.06.19.599732; this version posted June 28, 2025. The copyright holder for this preprint (which was not certified by peer review) is the author/funder, who has granted bioRxiv a license to display the preprint in perpetuity. It is made available under aCC-BY-NC 4.0 International license.

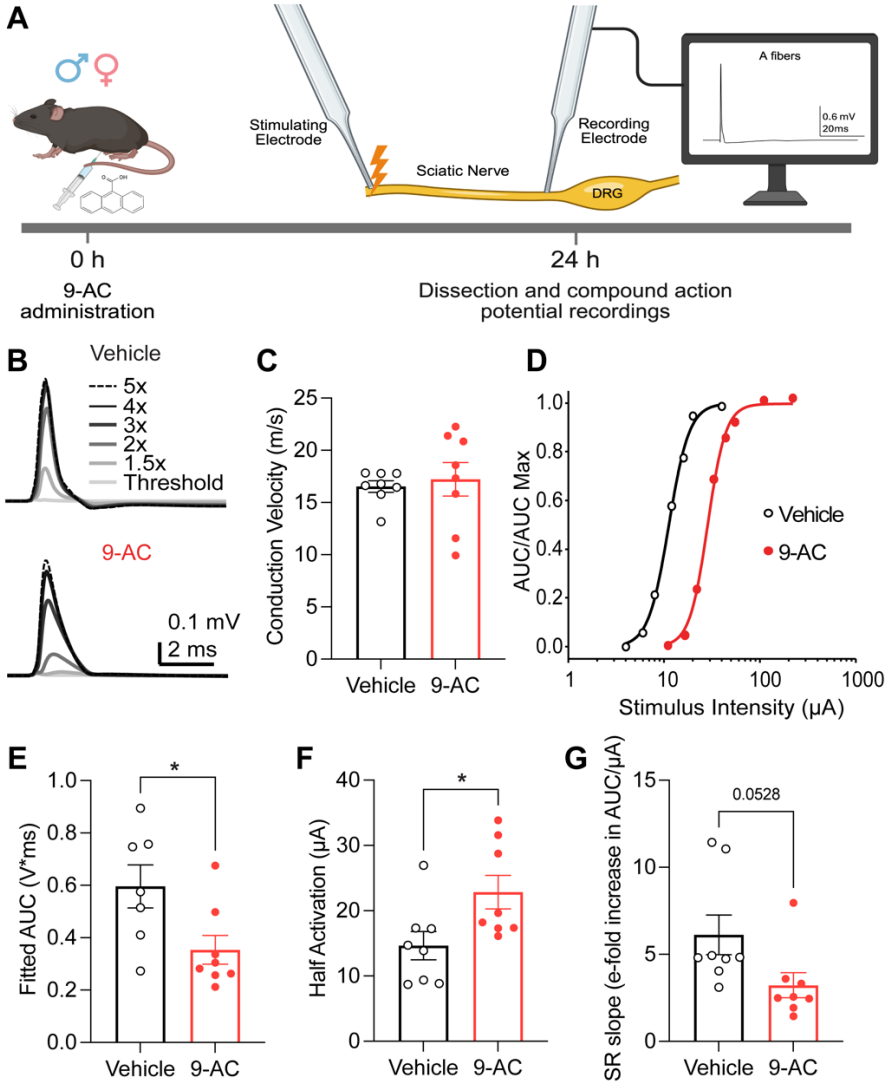

Figure 4. 9-AC reduces A-fiber compound action potential responses. (A) Schematic illustrating the experimental timeline. Mice received a single intraperitoneal injection of 9-AC (30 mg/kg), followed by sciatic nerve dissection 24 hours later. Compound action potential recordings were performed *ex vivo* to assess A-fiber function. **(B)** Representative traces showing responses to threshold and 1.5-5x threshold stimulation intensities in sciatic nerves from vehicle-treated (top) and 9-AC-treated (bottom) animals. **(C-G)** Quantification of (**C**) conduction velocity, (**D**) AUC/AUC max, (**E**) fitted AUC, (**F**) half activation, and (**G**) SR slope. Data in panels **C** and **E-G** were analyzed using the Welch's T test. Data are presented as mean ± SEM (n = 7-8 animals/group). Individual data points represent values from single animals (average of 2 nerves/animal). *p < 0.05.

bioRxiv preprint doi: https://doi.org/10.1101/2024.06.19.599732; this version posted June 28, 2025. The copyright holder for this preprint (which was not certified by peer review) is the author/funder, who has granted bioRxiv a license to display the preprint in perpetuity. It is made available under aCC-BY-NC 4.0 International license.

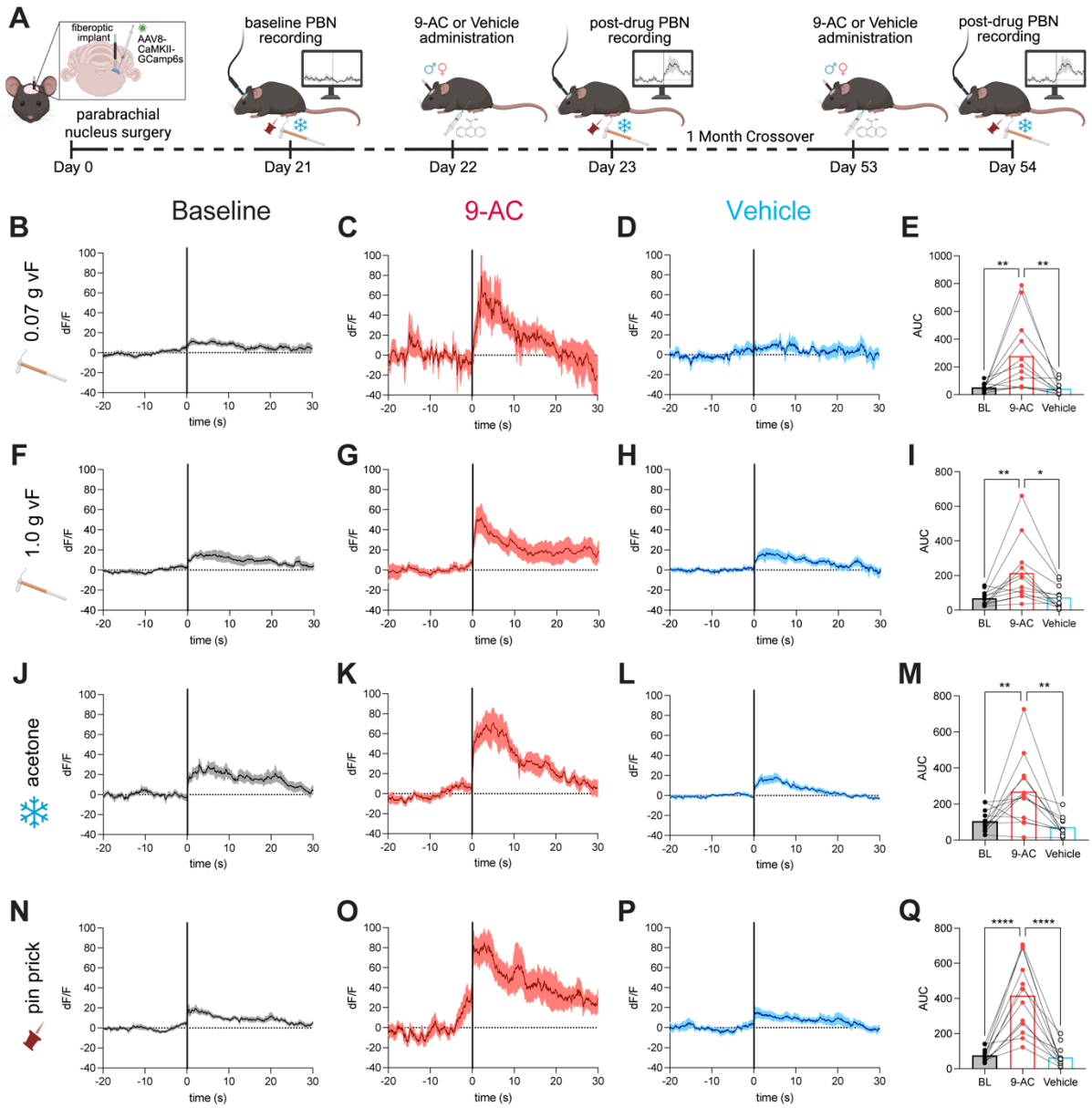

Figure 5. 9-AC increases parabrachial nucleus activity in response to somatosensory stimuli. (A) Schematic illustrating the experimental timeline. Mice received intra-parabrachial injections of AAV-GCaMP6s and were implanted with a fiberoptic cannula. Three weeks later, baseline *in vivo* fiber photometry recordings were performed. Mice then received a single intraperitoneal injection of 9-AC (30 mg/kg) or vehicle, followed 24 hours later by a second fiber photometry recording. One month later, a crossover was performed and the experiment was repeated. **(B-D)** Representative traces of normalized calcium-dependent fluorescence in response to a 0.07 g von Frey (vF) filament, and **(E)** quantification of the area under the curve (AUC). **(F-H)** Representative traces in response to a 1.0 g vF filament, and **(I)** corresponding AUC analysis. **(J-L)** Representative traces in response to acetone application, and **(M)** corresponding AUC analysis. **(N-P)** Representative traces in response to blunted pinprick stimulation, and **(Q)** corresponding AUC analysis. Data were analyzed using one-way ANOVA followed by Dunnett's post

bioRxiv preprint doi: https://doi.org/10.1101/2024.06.19.599732; this version posted June 28, 2025. The copyright holder for this preprint (which was not certified by peer review) is the author/funder, who has granted bioRxiv a license to display the preprint in perpetuity. It is made available under aCC-BY-NC 4.0 International license.

hoc test. Data are presented as mean ± SEM (n = 12 mice/group). Individual data points represent values from individual animals. *p < 0.05, **p < 0.01, ****p < 0.0001.

bioRxiv preprint doi: https://doi.org/10.1101/2024.06.19.599732; this version posted June 28, 2025. The copyright holder for this preprint (which was not certified by peer review) is the author/funder, who has granted bioRxiv a license to display the preprint in perpetuity. It is made available under aCC-BY-NC 4.0 International license.

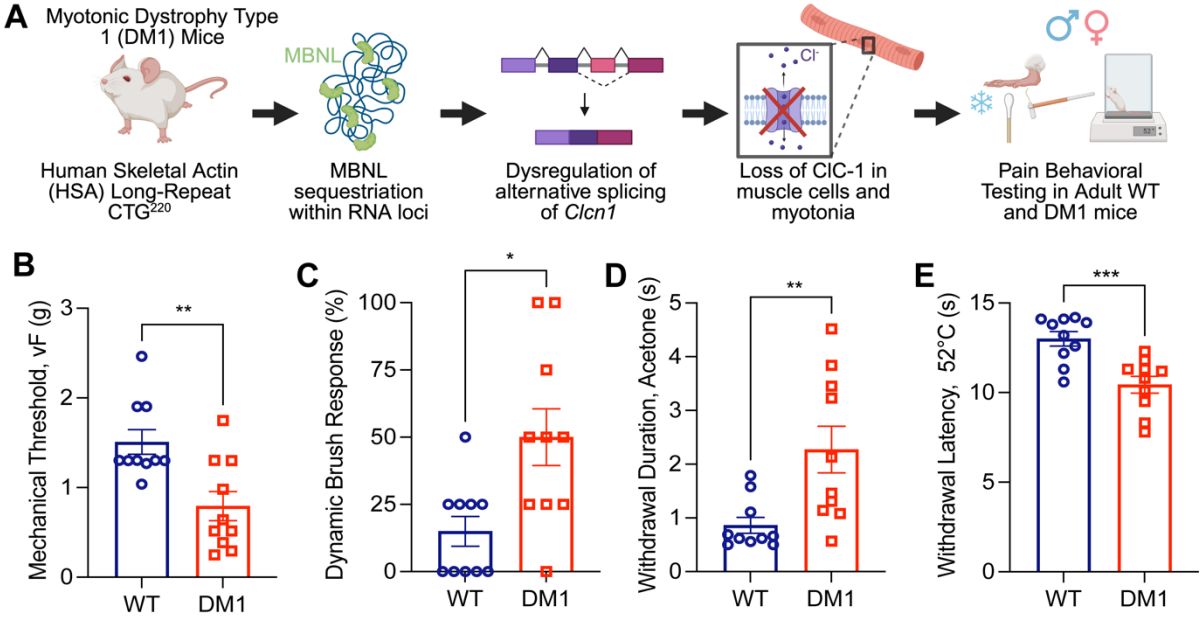

Figure 6. HSA LR20b myotonic dystrophy type 1 (DM1) mice exhibit nociplastic pain-like behavior. **(A)** Schematic illustrating the proposed mechanism by which expanded CTG repeats in the human skeletal actin (HSA) transgene of HSA LR20b mice lead to muscleblind-like protein (MBNL) sequestration, altered pre-mRNA splicing, and dysregulation of *Clcn1*. The resulting loss of ClC-1 chloride channel expression in skeletal muscle causes membrane hyperexcitability and myotonia. Adult wild-type (WT) FVB/N background mice and HSA LR20b (DM1) mice were assessed for pain-like behavior. **(B-E)** DM1 mice displayed significant hypersensitivity across multiple modalities: **(B)** static mechanical allodynia (von Frey test), **(C)** dynamic mechanical allodynia (brush stimulation), **(D)** cold allodynia (acetone application), and **(E)** thermal hyperalgesia (52 °C hot plate). Behavioral outcomes were analyzed using unpaired two-tailed Student's t tests. Data are presented as mean ± SEM (n = 10 mice/group). Individual data points represent values from individual animals. *p < 0.05, **p < 0.01, ***p < 0.001.

bioRxiv preprint doi: https://doi.org/10.1101/2024.06.19.599732; this version posted June 28, 2025. The copyright holder for this preprint (which was not certified by peer review) is the author/funder, who has granted bioRxiv a license to display the preprint in perpetuity. It is made available under aCC-BY-NC 4.0 International license.

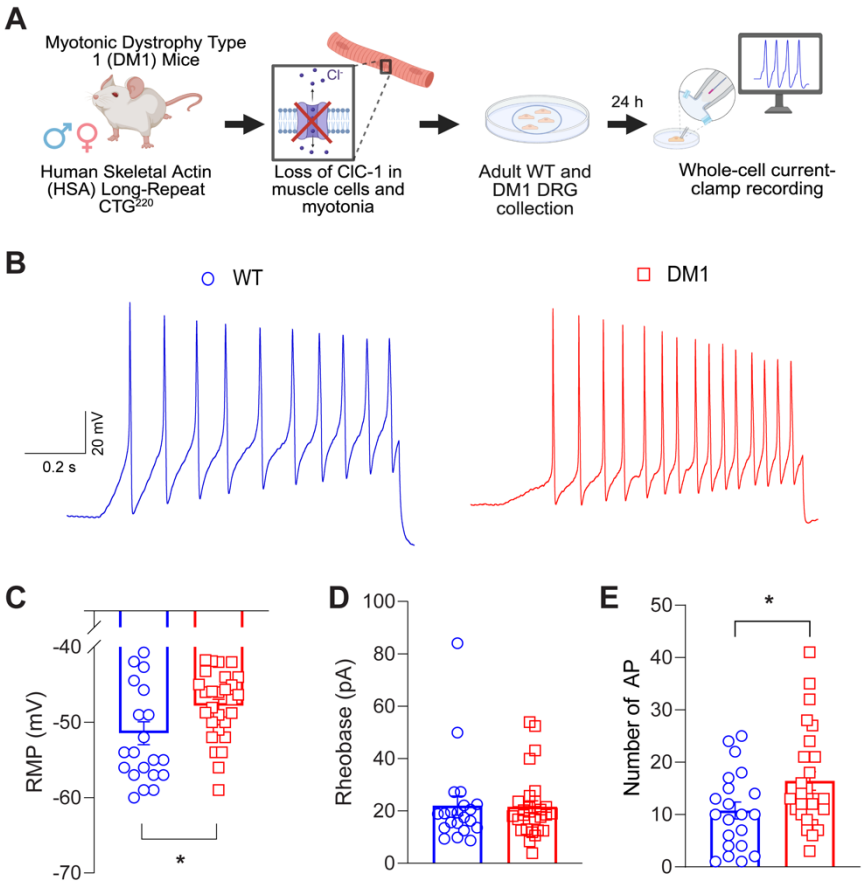

Figure 7. DM1 mice exhibit DRG neuron hyperexcitability. (A) Schematic illustrating the experimental timeline. Lumbar DRGs were dissociated from adult DM1 and wild-type (WT) mice. Whole-cell current-clamp recordings were performed in small- and medium-diameter DRG neurons. **(B)** Representative traces showing action potential (AP) firing in sensory neurons from WT (left) and DM1 (right) mice in response to suprathreshold current injection. **(C-E)** Quantification of **(C)** resting membrane potential, **(D)** rheobase, and **(E)** number of evoked APs. Data were analyzed using the Mann-Whitney U test. Data are presented as mean ± SEM (n = 21-28 neurons from 4 mice/group). Individual data points represent values from single neurons. *$p < 0.05$.

bioRxiv preprint doi: https://doi.org/10.1101/2024.06.19.599732; this version posted June 28, 2025. The copyright holder for this preprint (which was not certified by peer review) is the author/funder, who has granted bioRxiv a license to display the preprint in perpetuity. It is made available under aCC-BY-NC 4.0 International license.

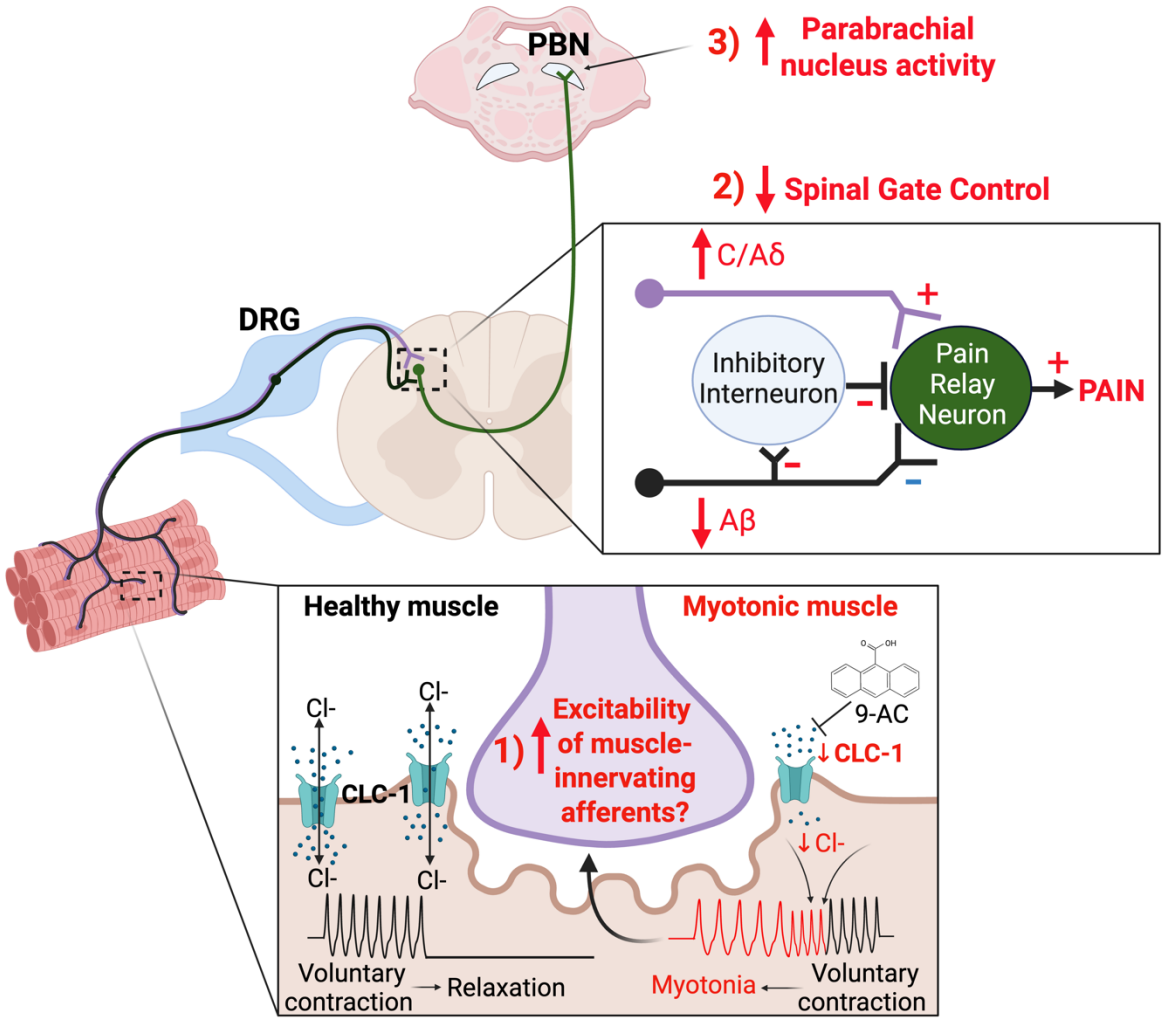

Figure 8. Schematic illustration of the proposed mechanisms by which myotonia leads to pain. The ClC-1 chloride channel is critical for maintaining the resting membrane potential of muscle fibers and facilitating their efficient repolarization following an action potential. In myotonia, loss or dysfunction of ClC-1 reduces chloride conductance, delays membrane repolarization, and prolongs muscle excitability. This results in repetitive, sustained contractions that drive hyperexcitability of the muscle membrane. We hypothesize that this chronic hyperexcitation of muscle initiates a cascade of changes within the pain pathway: (1) sensitization of muscle-innervating primary sensory afferents, (2) increased excitability of C-fiber nociceptors and decreased excitability of large-diameter myelinated afferents, thereby disrupting spinal gate control and amplifying pain transmission, and (3) increased bulk activity within the parabrachial nucleus, facilitating the central processing of pain. Together, these changes link the hyperexcitable muscle state characteristic of myotonia to the persistent pain observed in preclinical models and patients.

bioRxiv preprint doi: https://doi.org/10.1101/2024.06.19.599732; this version posted June 28, 2025. The copyright holder for this preprint (which was not certified by peer review) is the author/funder, who has granted bioRxiv a license to display the preprint in perpetuity. It is made available under aCC-BY-NC 4.0 International license.

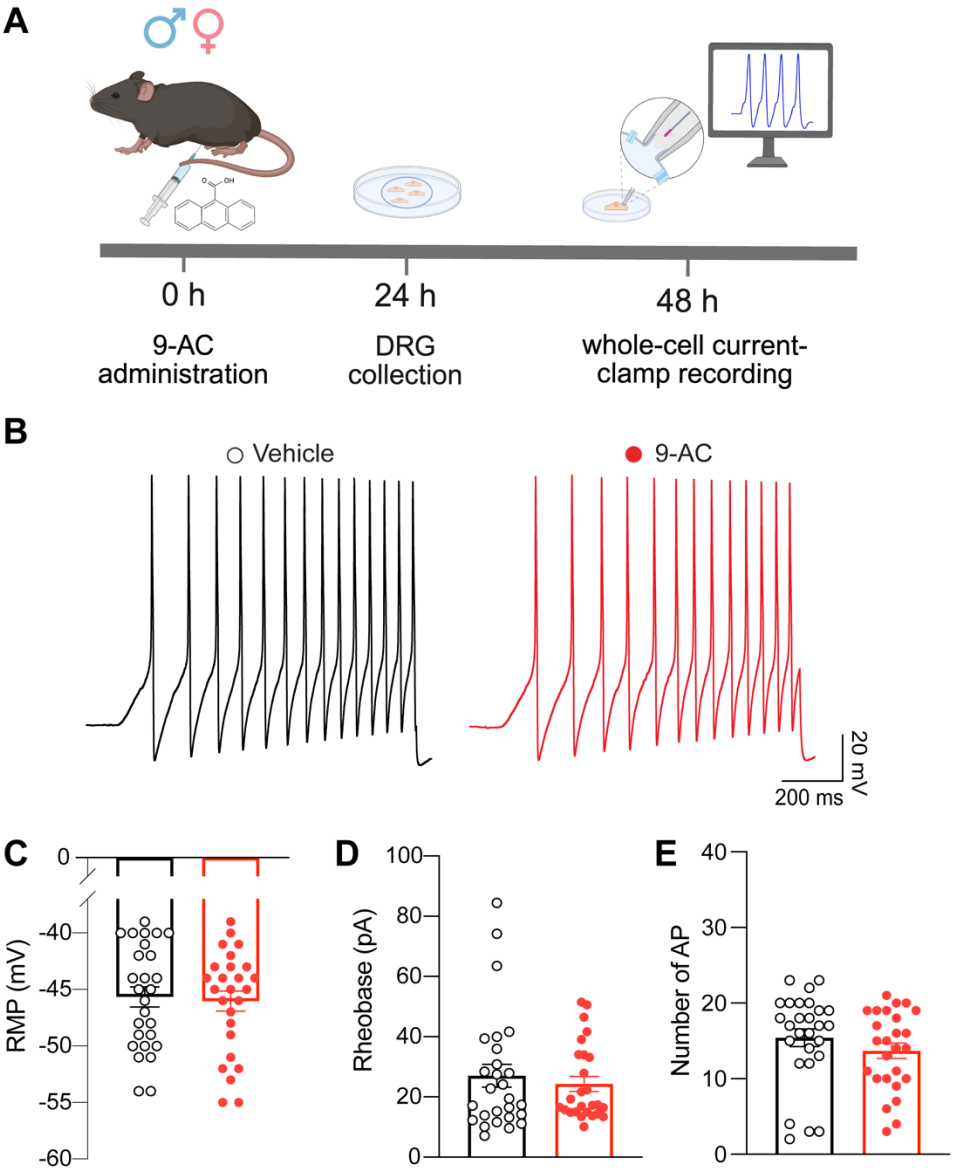

Supplemental Figure 1. 9-AC does not increase DRG neuron excitability 48 hours post-injection. **(A)** Schematic illustrating the experimental timeline. Mice received a single intraperitoneal injection of 9-AC (30 mg/kg), followed by lumbar DRG dissociation 24 hours later. Whole-cell current-clamp recordings were performed in small- and medium-diameter DRG neurons 48 hours post-injection. **(B)** Representative traces showing action potential (AP) firing in sensory neurons from vehicle-treated (left) and 9-AC-treated (right) animals in response to suprathreshold current injection. **(C-E)** Quantification of (**C**) resting membrane potential, (**D**) rheobase, and (**E**) number of evoked APs. (n=26-27 neurons from 4 mice per group). Data were analyzed using the Mann-Whitney U test. Data are presented as mean ± SEM. Individual data points represent values from single neurons.

bioRxiv preprint doi: https://doi.org/10.1101/2024.06.19.599732; this version posted June 28, 2025. The copyright holder for this preprint (which was not certified by peer review) is the author/funder, who has granted bioRxiv a license to display the preprint in perpetuity. It is made available under aCC-BY-NC 4.0 International license.

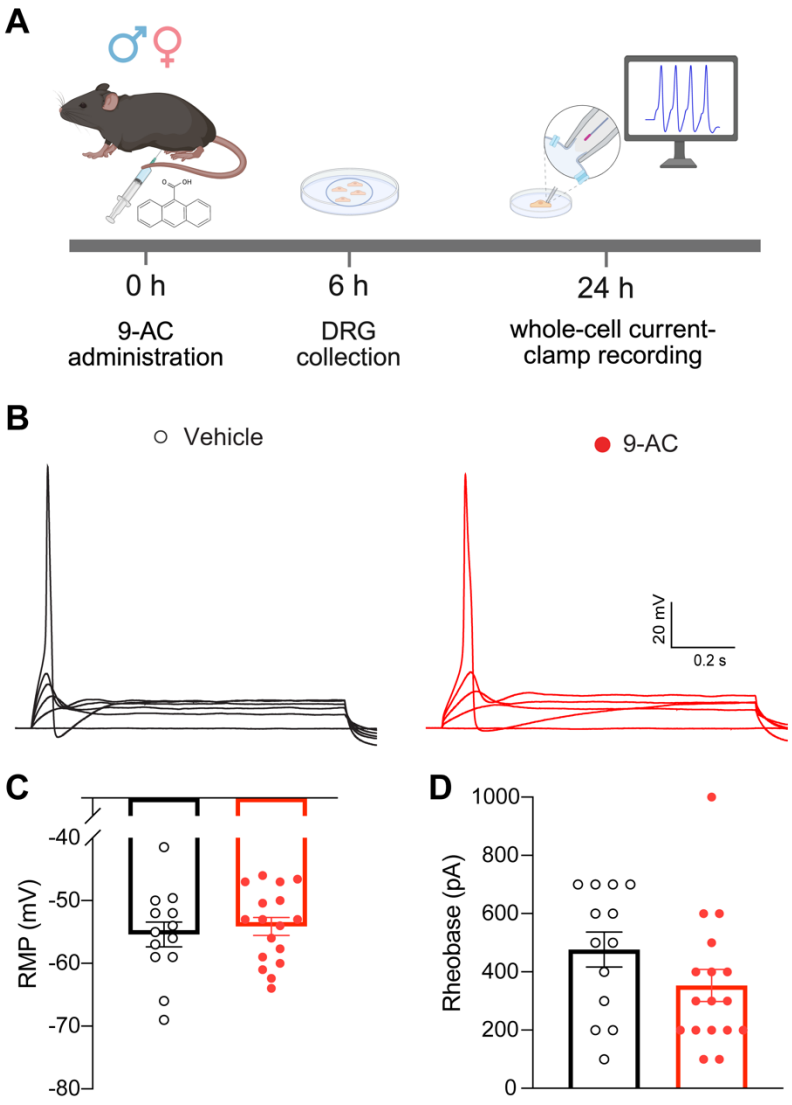

Supplemental Figure 2. Rheobase is not altered in large-diameter DRG neurons after 9-AC administration. (A) Schematic illustrating the experimental timeline. Mice received a single intraperitoneal injection of 9-AC (30 mg/kg), followed by lumbar DRG dissociation 6 hours later. Whole-cell current-clamp recordings were performed in large-diameter DRG neurons 24 hours post-injection. **(B)** Representative traces of current-clamp recordings showing rheobase in large-diameter DRG neurons from vehicle-treated and 9-AC-treated mice. **(C-D)** Quantification of **(C)** resting membrane potential and **(D)** rheobase, measured in 100 pA increments. Data were analyzed using the Mann-Whitney U test. Data are presented as mean ± SEM (n = 13-17 neurons from 4 mice/group). Individual data points represent values from single neurons.

bioRxiv preprint doi: https://doi.org/10.1101/2024.06.19.599732; this version posted June 28, 2025. The copyright holder for this preprint (which was not certified by peer review) is the author/funder, who has granted bioRxiv a license to display the preprint in perpetuity. It is made available under aCC-BY-NC 4.0 International license.

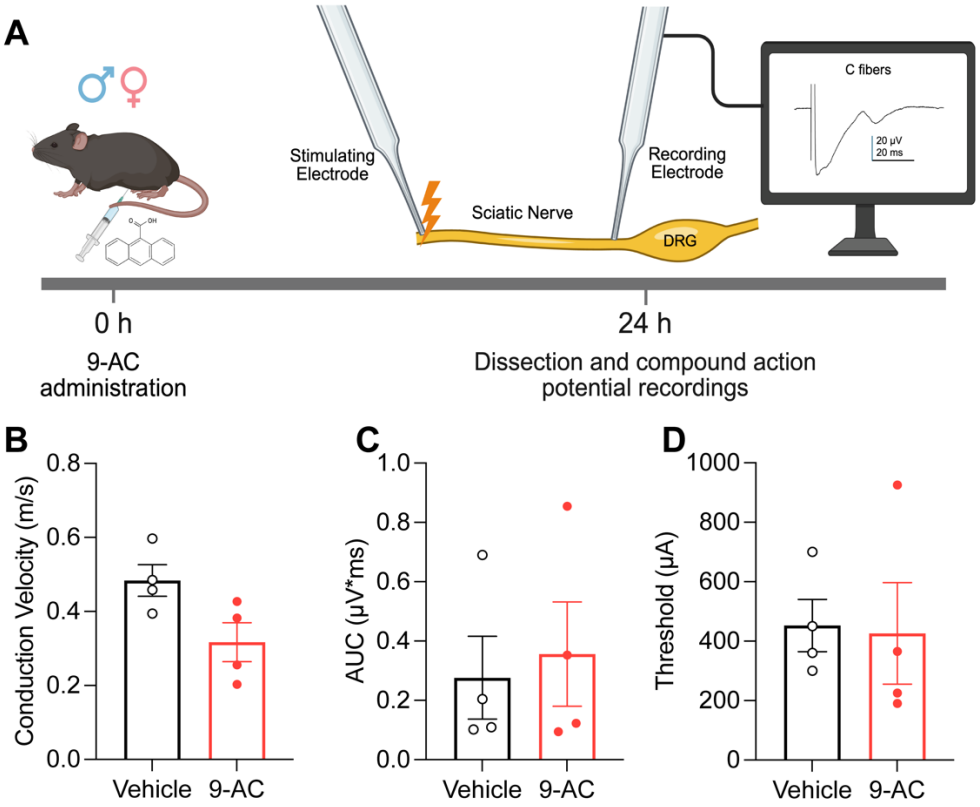

Supplemental Figure 3. 9-AC does not alter C-fiber compound action potential responses. (A) Schematic illustrating the experimental timeline. Mice received a single intraperitoneal injection of 9-AC (30 mg/kg), followed by sciatic nerve dissection 24 hours later. Compound action potential recordings were performed to assess C-fiber function. Quantification of (**B**) conduction velocity, (**C**) AUC, and (**D**) threshold. Data in panels **C-D** were analyzed using the Welch's T test. Data are presented as mean ± SEM (n = 4 animals/group). Individual data points represent values from single animals (average of 2 nerves/animal). *$p < 0.05$.

bioRxiv preprint doi: https://doi.org/10.1101/2024.06.19.599732; this version posted June 28, 2025. The copyright holder for this preprint (which was not certified by peer review) is the author/funder, who has granted bioRxiv a license to display the preprint in perpetuity. It is made available under aCC-BY-NC 4.0 International license.

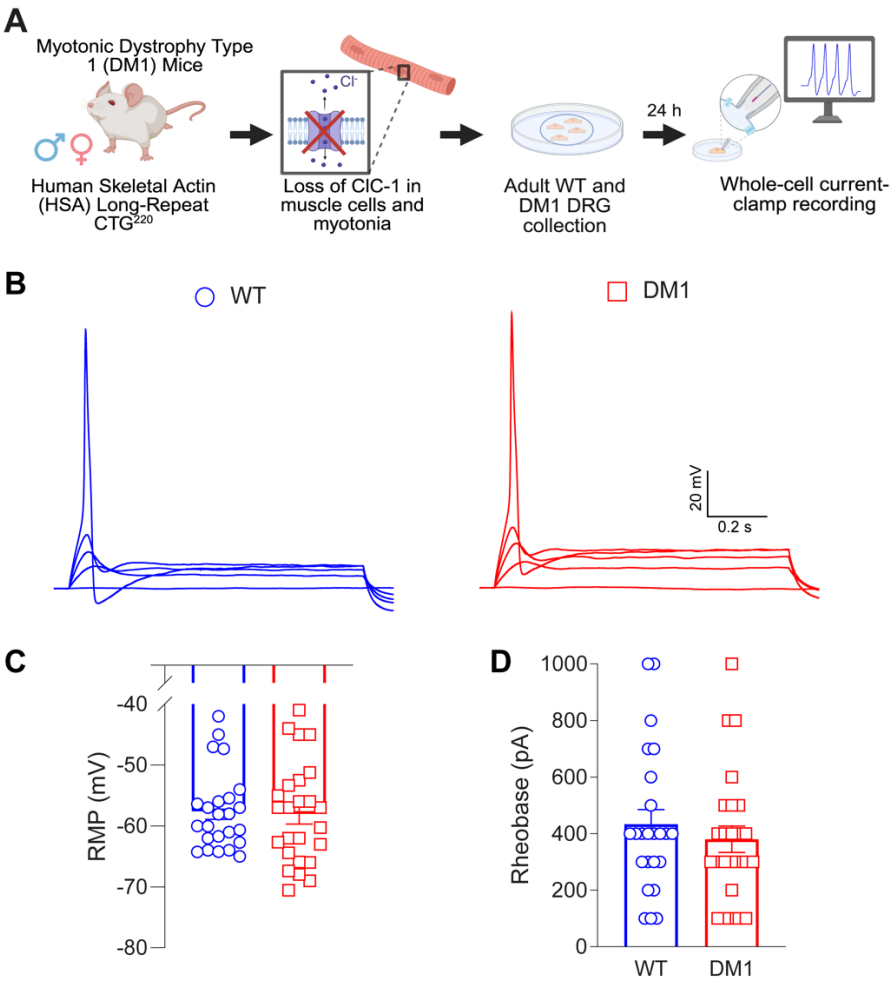

Supplemental Figure 4. Rheobase is not altered in in large-diameter DRG neurons from DM1 mice. **(A)** Representative traces of current-clamp recordings showing rheobase in large-diameter DRG neurons from wild-type (WT) control and HSA LR20b (DM1) mice. **(B-C)** Quantification of **(B)** resting membrane potential and **(C)** rheobase, measured in 100 pA increments, from large-diameter neurons recorded ex vivo 24 hours post-dissection. Data were analyzed using the Mann-Whitney U test. Data are presented as mean ± SEM (n = 24-25 neurons from 4 mice/group). Individual data points represent values from single neurons.